# Polarly localized WPR proteins interact with PAN receptors and the actin cytoskeleton during maize stomatal development

Qiong Nan[1], Si Nian Char[2], Bing Yang[2,3], Michelle R. Facette[1]

[1]Department of Biology, University of Massachusetts, Amherst, MA, 01003, USA
[2]Division of Plant Sciences, Bond Life Sciences Center, University of Missouri, Columbia, MO 65211, USA
[3]Donald Danforth Plant Science Center, St. Louis, MO 63132, USA

Correspondence: mfacette@umass.edu

**Orcid IDS:**
Q. Nan: orcid.org/0000-0002-9940-3015
M. Facette: orcid.org/0000-0002-6214-9359
S. N. Char: orcid.org/0000-0002-5759-0764
B. Yang: orcid.org/0000-0002-2293-3384

## ABSTRACT

Polarization of cells prior to asymmetric cell division is crucial for correctly orienting the cell division plane, and for subsequent cell fate and overall tissue patterning. In maize stomatal development, polarization of subsidiary mother cells prior to asymmetric division is controlled by the BRK-PAN-ROP pathway. Two catalytically inactive receptor-like kinases, PANGLOSS2 (PAN2) and PAN1, are polarized in subsidiary mother cells prior to division and required for correct division planes. Each of the proteins in the BRK-PAN-ROP pathway are polarized in subsidiary mother cells, with the polarization of each protein dependent on the previous one. Most of these proteins do not physically interact with one another, indicating there are likely unknown molecules in the pathway. We identified WEB1-PMI2 RELATED (WPR) proteins as new players during subsidiary mother cell polarization. WPRs physically interact with PAN2 and PAN1, and polarly accumulate in subsidiary mother cells at sites of guard mother cell contact. The polarized localization of WPR proteins depends on PAN2 but not PAN1. CRISPR-Cas9-induced mutations result in division plane defects in subsidiary mother cells, and mild overexpression of fluorescent protein tagged lines result in stomatal defects and alterations to the actin cytoskeleton. We further show that a subgroup of the WPR proteins directly interact with F-actin through their N-terminal domain. Our data implicate WPR proteins as potentially regulating actin filaments, which provides insight into their molecular function. Together, these results demonstrate WPR proteins as important for cell polarization and grass stomatal development.

## INTRODUCTION

Asymmetric cell division, which generates two daughter cells with different fates, is indispensable for cellular differentiation and diversity. In plants, cells do not move, therefore asymmetric cell division is particularly important for cellular patterning (De Smet and Beeckman, 2011; Muroyama and Bergmann, 2019). Certain processes are conserved during asymmetric cell division, although the specific molecular players may vary. A key principle of asymmetric cell division is cell polarization prior to mitosis, which is often marked by the polarization of plasma membrane–associated proteins and nuclear migration to the future division plane (Facette and Smith, 2012;

Galatis and Apostolakos, 2004; Yoshida et al., 2019). Cell polarization may be determined by intrinsic cues (pre-existing within the mother cell) or extrinsic cues (originating from outside the mother cell) (Yang 2008; Facette et al., 2018; Lipka et al., 2015).

The asymmetric division of maize subsidiary mother cells (SMCs) has been used as a model to understand cell polarization and asymmetric division in plants. Grasses such as *Zea mays* (maize), *Oryza spp* (rice) and *Brachypodium distachyon* (purple false brome) possess 4-celled stomatal complexes consisting of two guard cells flanked by a pair of subsidiary cells **(Supplemental Figure 1)**. Grass stomatal formation is initiated by an asymmetric division that generates a guard mother cell (GMC). The lateral neighbors of the GMC, called subsidiary mother cells (SMCs), divide asymmetrically to produce subsidiary cells that flank the GMC. It is proposed that SMC divisions are induced by an extrinsic cue from the GMC. Eventually, the GMC divides symmetrically to form a pair of guard cells flanked by the subsidiary cells (Stebbins and Shah, 1960; Facette and Smith, 2012; Raissig et al., 2017**;** Nunes et al., 2020; Gray et al., 2020).

In maize SMCs, several plasma membrane–associated proteins make up the BRK-PAN-ROP pathway, which promotes SMC polarity. BRICK1 (BRK1) is the earliest marker of SMC polarity (Facette et al., 2015). BRICK1 is a member of SCAR/WAVE complex that promotes branched actin networks via activation of the Arp2/3 complex (Frank and Smith 2002; Facette et al., 2015). BRK1, and all subsequent proteins, are polarized within SMCs, accumulating at the site of GMC contact. BRK1 is required for PANGLOSS2 (PAN2) and PAN1 polarization, which are two leucine-rich repeat receptor-like proteins with inactive kinase domains. PAN2 is required for the subsequent polarization of PAN1 (Zhang et al., 2012). Plant Rho family GTPase (ROP) is a small GTPase that physically interacts with PAN1 and its polarization is dependent on PAN1 (Humphries et al., 2011). After the polarized accumulation of these proteins, an actin patch appears at the SMC-GMC interface and the pre-mitotic SMC nucleus migrates towards the GMC. Within the pathway, only PAN1 and ROP have been shown to physically interact, however each protein is required for the next to be polarized. This implies that there are additional proteins important for the recruitment and/or polarization of each of the known players. Moreover, the molecular role that each of these proteins performs during SMC polarization is not known, including how polarization of these membrane-localized proteins culminates in nuclear migration and positioning of the division plane.

Since PAN1 and PAN2 are catalytically inactive kinases (Humphries et al., 2011; Zhang et al., 2012), it is unclear what their molecular function is. They may act as pseudokinases with important roles in scaffolding; however other than ROP no other PAN-interacting proteins have yet been characterized. In some cases, catalytically inactive receptors partner with active leucine rich repeat receptor kinases and act as inhibitors of function (Lee et al., 2012), but to date no active kinases have been identified in the pathway. PAN1 and PAN2 might perform functions similar to other polarized plasma membrane proteins and mediate diverse downstream functions that relate to cellular polarization such as: signal transduction, accumulation of other cell polarity factors, or eventual nuclear migration (De Smet and Beeckman, 2011; Ashraf and Facette, 2020). For example, in *A. thaliana* stomatal development, the polarized proteins BREAKING OF ASYMMETRY IN THE STOMATAL LINEAGE (BASL) and POLAR LOCALIZATION DURING ASYMMETRIC DIVISION AND REDISTRIBUTION (POLAR) act as scaffolding proteins for localized signal transduction (Dong et al., 2009; Pillitteri et al., 2011; Houbaert et al., 2018). Polarized BASL is required for pre-mitotic microtubule-based nuclear migration and post-mitotic actin-based nuclear migration (Muroyama et al., 2020). The LRRK INFLORESCENCE AND ROOT APICES RECEPTOR KINASE (IRK) is polarly localized

in root cells that divide (or have recently divided) asymmetrically however the molecular pathway downstream of IRK is not characterized (Campos et al., 2020).

Polarized accumulation of actin filaments is a prominent feature of maize SMC division, but the functional role of the actin patch that forms late in SMC polarization is unclear. While SMC nuclear migration in grasses is based on actin networks (Cho and Wick, 1990), formation of the actin patch and nuclear migration can be uncoupled (Cartwright et al., 2009; Apostolakos et al., 2018), implying that the actin patch has a function distinct from promoting nuclear migration. It is plausible that ROP GTPases are important for stimulating actin patch formation, however this has not been clearly demonstrated. In addition to the actin patch, there are other important actin-related processes during SMC polarization. The early role of BRK proteins, actin-mediated nuclear migration and actin patch formation imply multiple functions for actin networks in SMC polarization. SMC actin filaments may provide force or/and tracks for polarized organelle movement, and/or may facilitate endo/exocytosis at the polarity site (Hadley et al., 2006; Kimata et al., 2016; Wu and Bezanilla, 2018).

Actin-dependent movement of chloroplasts has been shown to involve WEAK CHLOROPLAST MOVEMENT UNDER BLUE LIGHT 1 (WEB1) and PLASTID MOVEMENT IMPAIRED 2 (PMI2) (Luesse et al., 2006; Kodama et al., 2010). WEB1, PMI2 and similar WEB1/PMI2-RELATED (WPR) proteins have DUF827 domain which is a series of coiled-coils; *A. thaliana* has fourteen DUF827-containing proteins including the WEB1-like (WEL) clade, PMI2-LIKE (PMI) clade and the WPRA and WPRB clades (Kodama et al., 2011). Previous studies in *A. thaliana* suggest proteins with this domain have diverse functions. WEB1 (Weak Chloroplast Movement under Blue Light 1) and PMI2 (Plastid Movement Impaired 2) are interacting proteins and are required for actin-based chloroplast photorelocation (Luesse et al., 2006; Kodama et al., 2010). TOUCH-REGULATED PHOSPHOPROTEIN1 (TREPH1) belongs to the WPRA protein clade, and is phosphorylated in response to touch (Wang et al., 2018). TREPH1 is required for touch-induced growth repression. WEB1 is membrane-associated and PMI2 is cytosolic in protoplasts, but *in planta* localization for DUF827 proteins has not been demonstrated. Moreover, while the demonstrated phenotypes of WEB1 and PMI2 implies an actin-related function, no evidence for physical or regulatory interactions with actin have been shown for any DUF827 protein thus far.

In this study, we identified members of the DUF827 domain-containing WPR protein family that participate in maize SMC polarization. WPRs interact with both PAN2 and PAN1, and WPRs can also form homodimers and heterodimers. WPRs localize polarly in SMC at sites of guard mother cell (GMC) contact, and their polarized localization depends on PAN2 but not PAN1. These findings suggest WPRs are plasma membrane-associated proteins that are important for pre-mitotic polarity in maize SMCs, and are the first physical link between PAN1 and PAN2. CRISPR-Cas9-induced *wprb1;wprb2* double mutants and plants ectopically expressing WPRB2 have an increased frequency of aberrantly formed subsidiary cells. WPRB2 overexpression causes a decrease in cellular F-actin. Additionally, we show that WPRB2 directly interacts with F-actin through its N-terminus. In total, these results suggest the WPRs are components of the BRK-PAN-ROP pathway and likely act downstream of PAN2 to regulate actin-associated processes during cell polarization.

## RESULTS

### WPRs Exhibit Polarized Localization in Maize SMCs

Previously, four related proteins containing Domain of Unknown Function 827 (DUF827) were identified as PAN2 interactors by Co-IP/MS (M. Facette, A. Fulzele, E. Bennett & L.G. Smith, Unpublished data). The DUF827 family includes previously identified WEB1-PMI2 RELATED (WPR) proteins (Kodama et al., 2010; Gardiner et al., 2011; Kodama et al., 2011). We identified sixteen WPRs in *A. thaliana* and seventeen WPRs in maize. a gene tree was inferred, and these **(Supplemental Figure 2)** proteins fall into five clades: WPRA, PMI, WEB/WEL, WPRB and WPRC. The four maize proteins interacting with PAN2 fall into WPRA and WPRB clades; we named these proteins WPRA1, WPRA2, WPRB1, and WPRB2. WPRs have predicted coiled-coil domains in their central plant-specific DUF827 region, flanked by uncharacterized N- and C-terminal regions.

Thus far, all proteins identified in the BRK-PAN-ROP pathway polarly localize in SMCs prior to division (Cartwright et al., 2009; Humphries et al., 2011; Zhang et al., 2012; Facette et al., 2015). To determine if WPR proteins play a role in SMC polarization, we determined if they were similarly polarized. We created stable transgenic maize lines expressing either WPRA2-CFP or WPRB2-RFP. Genomic fragments containing the native promoter, introns and terminator were used. At early stages of stomatal development prior to SMC formation, WPRA2-CFP **(Figure 1A)** and WPRB2-RFP **(Figure 1B)** localize to the cell periphery in all cell types. WPRB2-RFP is enriched in cell corners, similar to BRK1-CFP (Facette et al., 2015). As development proceeds, WPRA2-CFP and WPRB2-RFP become enriched in the SMC at the contact of GMC contact and remain polarized after SMC division **(Figure 1)**. Plasmolysis experiments confirm that WPRA2-CFP and WPRB2-RFP are polarized in the SMC, not the GMC **(Supplemental Figure 3)**. Thus, the localization of WPRA2 and WPRB2 is similar to known BRK-PAN-ROP pathway components and supports a role in SMC polarization.

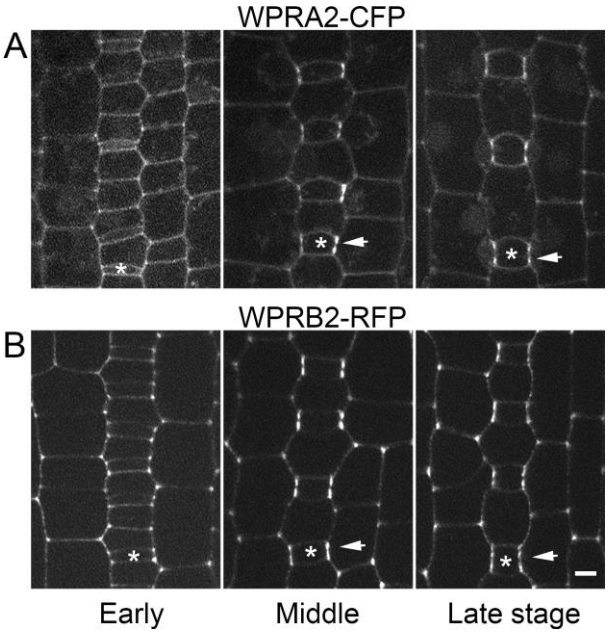


**Figure 1. WPRA2-CFP and WPRB2-RFP polarize in developing subsidiary mother cells.** The stomatal division zone of the fourth of transgenic maize plants was dissected and analyzed. Three different stomatal development stages were selected according to GMC width and SMC division status to observe the localization of WPRA2-CFP (A) and WPRB2-RFP (B). Arrows point to sites of WPRA2-CFP or WPRB2-RFP accumulation in SMCs where they contact the adjacent GMC. Asterisks mark a GMC within each stomatal row. Scale bar = 5 µm.

Notably, WPR proteins contain no predicted transmembrane domains or lipidation signals, indicating their association with the membrane is either peripheral or via interactions with other membrane proteins.

## WPRs Interact with PAN1 and PAN2

To confirm the WPR-PAN2 interaction, we performed co-immumoprecipitation/mass spectrometry (co-IP/MS) experiments using three strategies, using either our fluorescent protein fusion lines or a native antibody. Firstly, we used anti-GFP to immunoprecipitate WPRA2 from transgenic plants expressing WPRA2-CFP; non-transgenic wild type plants were used as a negative control. Secondly, we used anti-RFP to immunoprecipitate WPRB2 from transgenic plants expressing WPRB2-

RFP, again using non-transgenic plants as a negative control. Thirdly, we used an antibody raised against WPRA1/A2 (see Methods, and **Supplemental Fig. 4**) to pull down endogenous WPRA from non-transgenic plant extracts, with reactions omitting this antibody

as a negative control. In each experiment, three biological replicates were performed. After comparing relative abundances of identified proteins with

corresponding negative controls, we found WPRA family proteins co-precipitated with WPRB family proteins in all three assays (**Table 1 and Supplement Data Set 1**). Moreover, we found that both PAN1 and PAN2 co-precipitated with WPRA1/A2 and PAN2 co-precipitated with WPRB2-RFP.In addition, enrichment of WPRB3 peptides was detected in WPRA2-CFP and WPRA1/A2 immunoprecipitates, suggesting WPRB3 may also associate with WPRA proteins.

To validate these interactions, and test whether WPRs directly interact with PAN1 and PAN2, yeast two-hybrid assays were conducted using intracellular portions of PAN1

and PAN2 as bait (Zhang et al., 2012), and WPRA1, WPRA2, WPRB1, WPRB2, and WPRB3 as prey. In these assays, no interaction between WPRA1 or WPRA2 and PAN1 or PAN2 was observed. However, we found that both WPRB1 and WPRB2 interact with PAN1 and PAN2. WPRB3 interacts with PAN2 but not PAN1 **(Figure 2A and 2B)**. These data confirm a direct physical interaction between the intracellular regions of PAN and WPRB proteins. Our co-IP MS data suggest

| | Gene ID | Gene name | Rep1 # Unique Peptides | Rep2 # Unique Peptides | Rep3 # Unique Peptides | Control 1 # Unique Peptides | Control 2 # Unique Peptides | Control 3 # Unique Peptides |
|---|---|---|---|---|---|---|---|---|
| Anti-GFP | Zm00001d041088 | **WPRA2 (bait)** | 28 | 42 | 2 | 2 | 0 | 0 |
| | Zm00001d007164 | WPRB2 | 5 | 3 | 0 | 0 | 0 | 0 |
| | Zm00001d010610 | WPRB3 | 15 | 13 | 0 | 0 | 0 | 1 |
| | Zm00001d029420 | WEB subfamily protein | 5 | 7 | 0 | 0 | 0 | 0 |
| Anti-WPRA1/A2 | Zm00001d023629 | **WPRA1 (bait)** | 24 | 19 | 26 | 0 | 1 | 2 |
| | Zm00001d041088 | **WPRA2 (bait)** | 26 | 19 | 27 | 0 | 0 | 0 |
| | Zm00001d047516 | WPRB1 | 5 | 4 | 6 | 0 | 0 | 0 |
| | Zm00001d007164 | WPRB2 | 19 | 21 | 21 | 0 | 0 | 0 |
| | Zm00001d010610 | WPRB3 | 24 | 21 | 24 | 0 | 1 | 0 |
| | Zm00001d026193 | WPRC subfamily protein | 2 | 1 | 0 | 0 | 0 | 0 |
| | Zm00001d000443 | WPRC subfamily protein | 2 | 2 | 0 | 0 | 0 | 1 |
| | Zm00001d048523 | WEB subfamily protein | 2 | 2 | 2 | 0 | 0 | 0 |
| | Zm00001d007862 | PAN2 | 4 | 5 | 4 | 0 | 0 | 2 |
| | Zm00001d031437 | PAN1 | 2 | 5 | 2 | 0 | 0 | 0 |
| Anti-RFP | Zm00001d007164 | **WPRB2 (bait)** | 18 | 20 | 17 | 0 | 1 | 0 |
| | Zm00001d023629 | WPRA1 | 15 | 16 | 16 | 0 | 0 | 0 |
| | Zm00001d041088 | WPRA2 | 18 | 21 | 20 | 0 | 2 | 0 |
| | Zm00001d010610 | WPRB3 | 1 | 2 | 1 | 0 | 0 | 0 |
| | Zm00001d007862 | PAN2 | 3 | 0 | 1 | 0 | 0 | 0 |

**Table 1**. **WPR proteins interact with other WPR family members and PAN receptors.** WPR-interacting proteins identified by Co-IP/MS. For a complete list of all proteins, see **Supplementary Data Set 1**. Three different experiments were performed. 1: Anti-GFP was used to pull down WPRA2 and interacting proteins from extracts of plants expressing WPRA2-CFP, and from non-transgenic plants as a negative control. 2: Anti-WPRA1/A2 was used to pull down WPRA1/A2 and interacting proteins from B73 extracts; negative controls used the same extracts but omitted the anti-WPRA1/A2 antibody. 3: Anti-RFP was used to pull down WPRB2 and interactors from extracts of plants expressing WPRB2-RFP, and from non-transgenic plants as a negative control. B73 v4 gene codes are used to identify proteins, and the number of unique peptides (# peptides) is listed. The baits WPRA2, WPRA1/A2, and WPRB2 are highlighted in bold

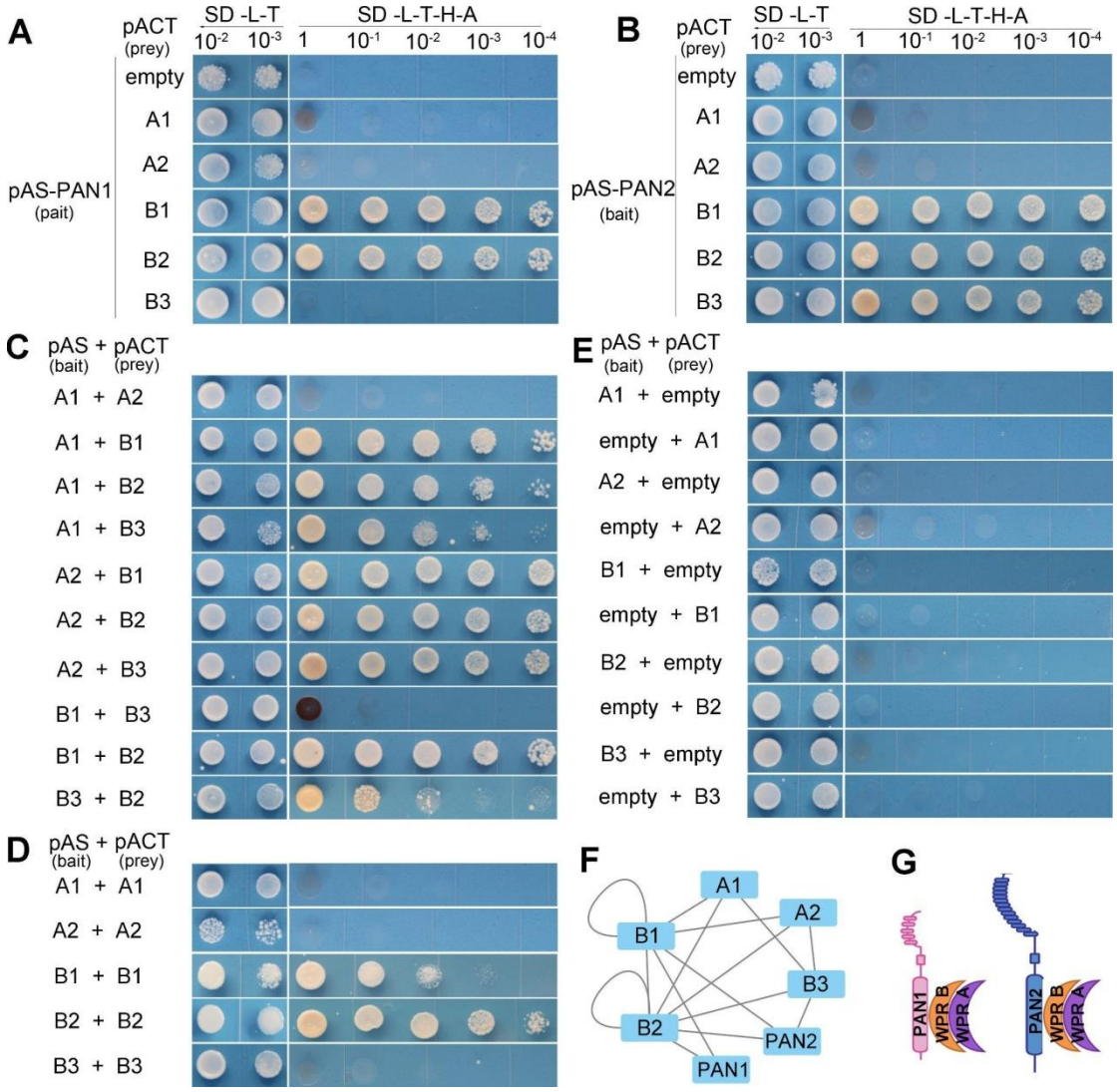


**Figure 2. Yeast 2-hybrid analysis of WPR and PAN protein interactions.** Interactions were assessed using the GAL4-based yeast two-hybrid system. Yeast was grown at different dilutions on non-selective (-L-T) and selective (-L-T-A-H) media. Soluble intracellular regions of PAN1 and PAN2 were used. **(A)** and **(B)**, interactions of PAN1 and PAN2 with WPRA1, WPRA2, WPRB1, WPRB2, and WPRB3. **(C)** Heterodimer formation was assessed between WPRA1, WPRA2, WPRB1, WPRB2, and WPRB3. **(D)** Homodimer formation was assessed between WPRA1, WPRA2, WPRB1, WPRB2, and WPRB3. **(E)** Negative controls using empty bait plasmid pASGW-attR or prey plasmid pACTGW-attR. **(F)** Network diagram showing the observed interactions between WPRs and PAN1/PAN2. **(G)** A model of protein complex formation between PAN and WPR proteins.

WRPA-WPRB interact, and previous work has shown that *A. thaliana* WEB1 interacts with and PMI2 and itself (Kodama et al., 2010). We performed yeast 2-hybrid assays to determine if maize WPR proteins also form homo/heterodimers, and found several hetero- and homo-dimer combinations **(Figure 2C and 2D)**. This includes heterodimers between WPRA and WPRB proteins. This potentially explains why Co-IP/MS data indicates that PAN proteins interact with both WPRA and WPRB proteins, but no direct interaction between WPRA and PAN proteins was observed. Taken together, the Co-IP/MS combined with Y2H assays demonstrated an interaction network **(Figure 2F).** We propose that WPRA-WPRB heterodimers interact with both PAN1 and PAN2 receptors, with WPRB mediating both interactions **(Figure 2G)**.

## WPR Proteins Act after PAN2 but before PAN1 in the BRK-PAN-ROP Pathway

Previous studies have demonstrated that BRK-PAN-ROP pathway components polarize sequentially in SMCs the following order: BRK1, PAN2, PAN1, followed by formation of a cortical F-actin patch at the GMC contact site (Humphries et al., 2009; Zhang et al, 2012; Facette et al., 2015; **Supplemental Figure 1B**). To determine the timing of WPRA2-CFP and WPRB2-RFP polarization, we examined SMCs in plants co-expressing either WPRA2-CFP or WPRB2-RFP with BRK1-CFP, PAN2-YFP, PAN1-YFP, and the actin marker FABD2-YFP. Quantitative analyses of the co-expression data are in **Supplemental Table 1**. In plants co-expressing BRK1-CFP and WPRB2-RFP, 0/326 SMCs showed polarization of only WPRB2-RFP, while 94/326 SMCs showed polarization of only BRK1–CFP, indicating that BRK1-CFP polarizes prior to WPRB2-RFP **(Figure 3A)**. In plants co-expressing WPRA2-CFP and WPRB2-RFP, we observed 276 SMCs, and in all cells WPRA2-CFP and WPRB2-RFP co-localized at the same time **(Figure 3B)**. This is consistent with WPRA and WPRB proteins acting as a heterodimer. In PAN2-YFP (n=254) **(Figure 3C)** or PAN1-YFP (n = 286) **(Figure 3D)**, and WPRA2-CFP and co-expressing SMCs SMCs always showed co-polarization of WPRA2–CFP and PAN2-YFP/PAN1-YFP at the GMC contact site. Finally, in WPRA2-CFP and FABD2-YFP co-expressing plants, 0/207 SMCs had polarized FABD2-YFP only, while 67/207 had polarized WPRA2-CFP only, **(Figure 3E)**, suggesting WPRA2 polarizes prior to the actin patch in developing SMCs. Thus, WPRA2-CFP and WPRB2-RFP polarize after BRK1-CFP, but prior to actin.

To investigate the possible dependence of WPR polarization on the functions of known BRK-ROP-PAN pathway components, we examined the polarization of WPRA2-CFP and WPRB2-RFP in *brk1,pan1* and *pan2* mutants **(Figure 4)**. In *brk1* mutants, both WPRA2-CFP and WPRB2-RFP lost their polarized accumulation at the SMC-GMC interface (Figure 4A and 4B). This is consistent with the

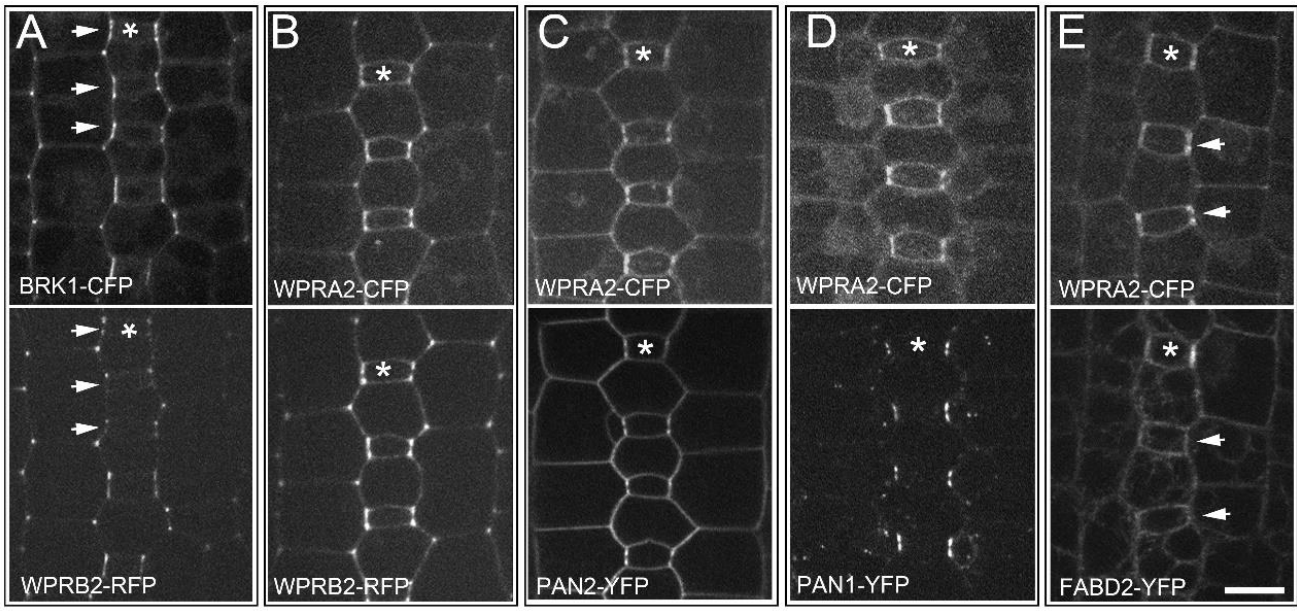


**Figure 3. WPR proteins polarize in SMCs after BRK1 and before actin.** Plants co-expressing BRK1-CFP & WPRB2-RFP **(A)**, WPRA2-CFP & WPRB2-RFP **(B)**, WPRA2-CFP & PAN1-YFP **(C)**, WPRA2-CFP & PAN2-YFP **(D)**, or WPRA2-CFP and FABD2-YFP **(E)** were analyzed during stomatal development. Top and bottom panels are the same cells, imaged on different channels. Asterisks mark the top GMC in each panel. Fluorescent proteins were scored as polarized when fluorescence was brighter at the SMC-GMC interface than adjacent portions of the cell periphery. Arrows in **(A)** mark examples of cells in which BRK1-CFP is polarized, but not WPRB2-RFP. Arrows in **(E)** marker examples of cells in which WPRA2-CFP is polarized but not FABD2-YFP. Quantification of co-expression is in **Supplemental Table 1.** Scale bar = 10 µm.

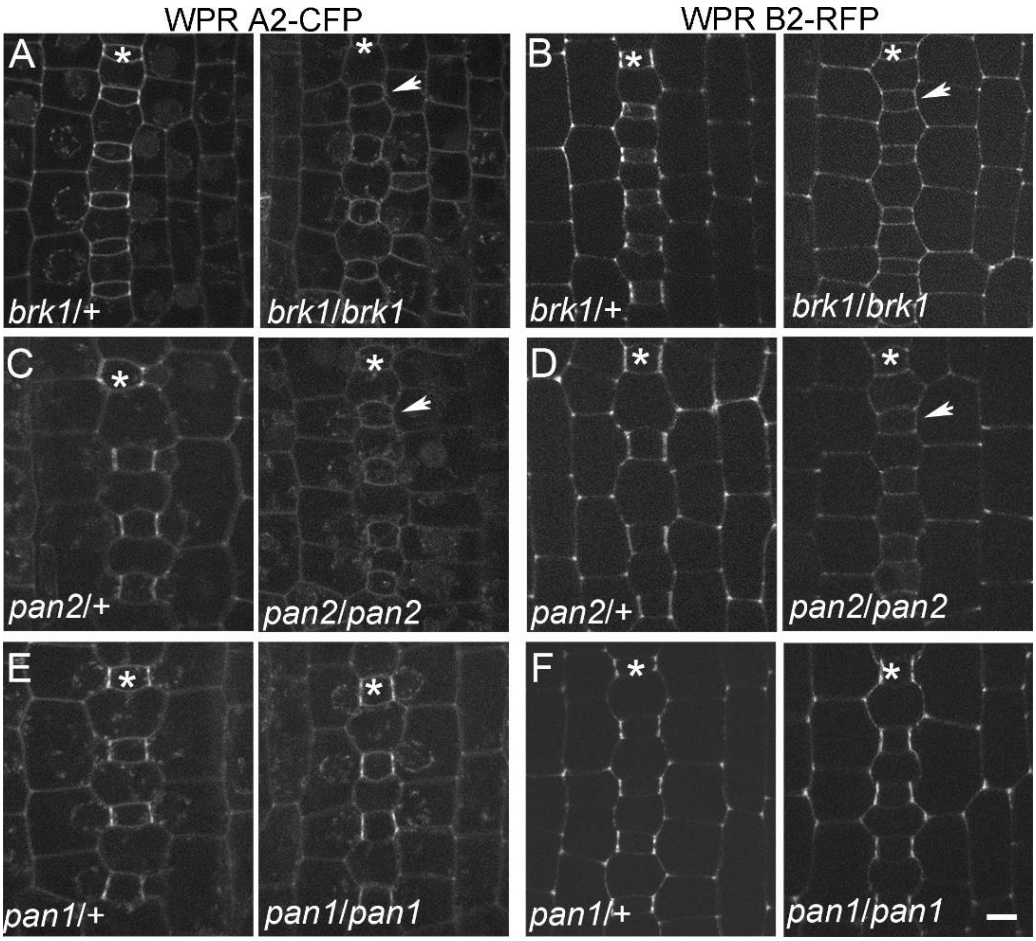


**Figure 4**. **Polarization of WPR proteins depends on BRK1 and PAN2, but not PAN1.** Localization of WPRA2-CFP and WPRB2-RFP in *brk1*, *pan2* and *pan1* mutants and non-mutant siblings was analyzed in developing leaf 4. WPRA2-CFP **(A)** and WPRB2-RFP **(B)** in developing stomata of *brk1* mutants and non-mutant (heterozygous) siblings. WPRA2-CFP **(C)** and WPRB2-RFP **(D)** in developing stomata of *pan2* mutants and non-mutant (heterozygous) siblings. WPRA2-CFP **(E)** and WPRB2-RFP **(F)** in developing stomata of *pan1* mutants and non-mutant (heterozygous) siblings. Asterisks mark GMC rows. Arrows point to SMCs without polarized localization of WPRA2-CFP or WPRB2-RFP. 3-6 plants of each genotype were used for data collection. Scale bar, 5 µm.

co-localization data, and indicates that WPRs are downstream of BRK1. Polarized localization of both WPRA2-CFP and WPRB2-RFP at the GMC contact site of SMCs is completely lost in *pan2* mutants **(Figure 4C and 4D)**, but remains polarized in *pan1* mutants **(Figure 4E and 4F)**. Thus, although we observed no timing difference in the polarized accumulation of PAN2, PAN1 and WPR proteins, PAN2 acts genetically upstream of WPRs and promotes their polarized accumulation. In contrast, PAN1, which acts downstream of PAN2, is not required for WPR polarization.

## CRISPR/Cas9-Mediated Knockout of *Wprb1* and *Wprb2* Causes Subsidiary Cell Defects

To determine whether WPRs are required for asymmetric cell division during maize stomatal development, we used CRISPR/Cas9 to generate *wpr* mutants. The coding sequences of *Wpra1* and *Wpra2* are 92% identical, therefore both genes were targeted using the same two guide RNAs. *Wprb1* and *Wprb2* are 57% identical, and therefore two different guide RNAs were used in a single construct to separately target the two genes. Single mutants were identified for

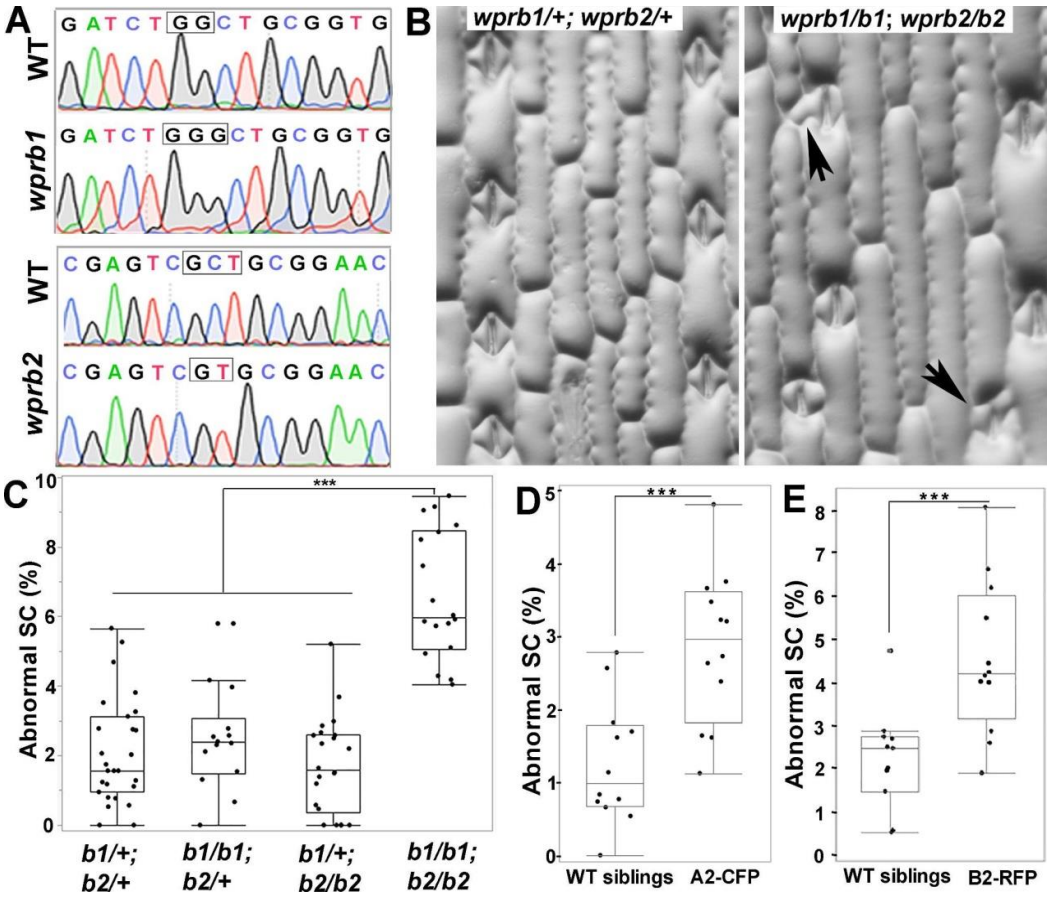


**Figure 5. CRISPR-Cas9 induced *wprb1*;*wprb2* double mutants and WPRA2-CFP and WPRB2-RFP overexpression lines have SC defects. (A)** Cas9-edited *Wprb1* and *Wprb2* genes. Mutated regions in the are labeled in black square.These mutations cause frameshifts and premature termination. **(B)** Representative image of the third leaf epidermis of *wprb1*/+; *wprb2*/+ and *wprb1*/*wprb1*; *wprb2*/*wprb2* mutants. Black arrows indicate abnormal subsidiary cells. **(C)** Quantification of abnormal subsidiary cells (SC) in *wprb1*/+; *wprb2*/+ (n = 27 plants), *wprb1*/*b1*;*wprb2*/+ (n = 14 plants), *wprb1*/+;*wprb2*/*wprb2* (n = 22 plants) and *wprb1*/*wprb1*;*wprb2*/*wprb2* (n=18 plants). For each plant 100-200 subsidiary cells were examined. p-value from Student's T-test comparing each genotypes, ***P≤ 0.001. **(D)** and **(E)** Quantification of abnormal subsidiary cells in WPRA2-CFP or WPRB2-RFP expressing plants and non-transgenic siblings grown in parallel. (n = 11-12 plants and about 120-200 cells per genotype). Student's T-test were performed, ***p≤ 0.001.

each gene **(Supplemental Figure 5A-C).** The edited lines were backcrossed with B73 and the transgene was segregated away. Single mutants were then crossed to obtain true-breeding double mutant lines. Despite PCR and Sanger sequence genotyping of many hundreds of plants from several different crosses, we never recovered *wpra1;wpra2* double homozygous mutants (**Supplemental Figure 5D**). This might reflect an essential shared function for the two genes in the male gametophyte, based on the high expression level of *wpra1* and *wpra2* in maize pollen (**Supplemental Figure 5E**). We were, however, able to generate *wprb1;wprb2* double homozygous mutants by crossing *wprb1/wprb1; wprb2/+* x *wprb1/+; wprb2/wprb2* plants (which generate double mutants at a higher frequency than a selfed double heterozygote). No stomatal phenotypes were observed in *wprb1* or *wprb2* single homozygotes, however *wprb1/wprb1; wprb2/wprb2* double mutants have an increased percentage of defective subsidiary cells relative to *wprb1/+;wprb2/+*, *wprb1/b1;wprb2/+ and wprb1/+;wprb2/b2* siblings (**Figure 5**). Since the aberrant SC phenotype of *wprb1;wprb2* double mutants is mild relative to *pan1* or *pan2* mutants, we

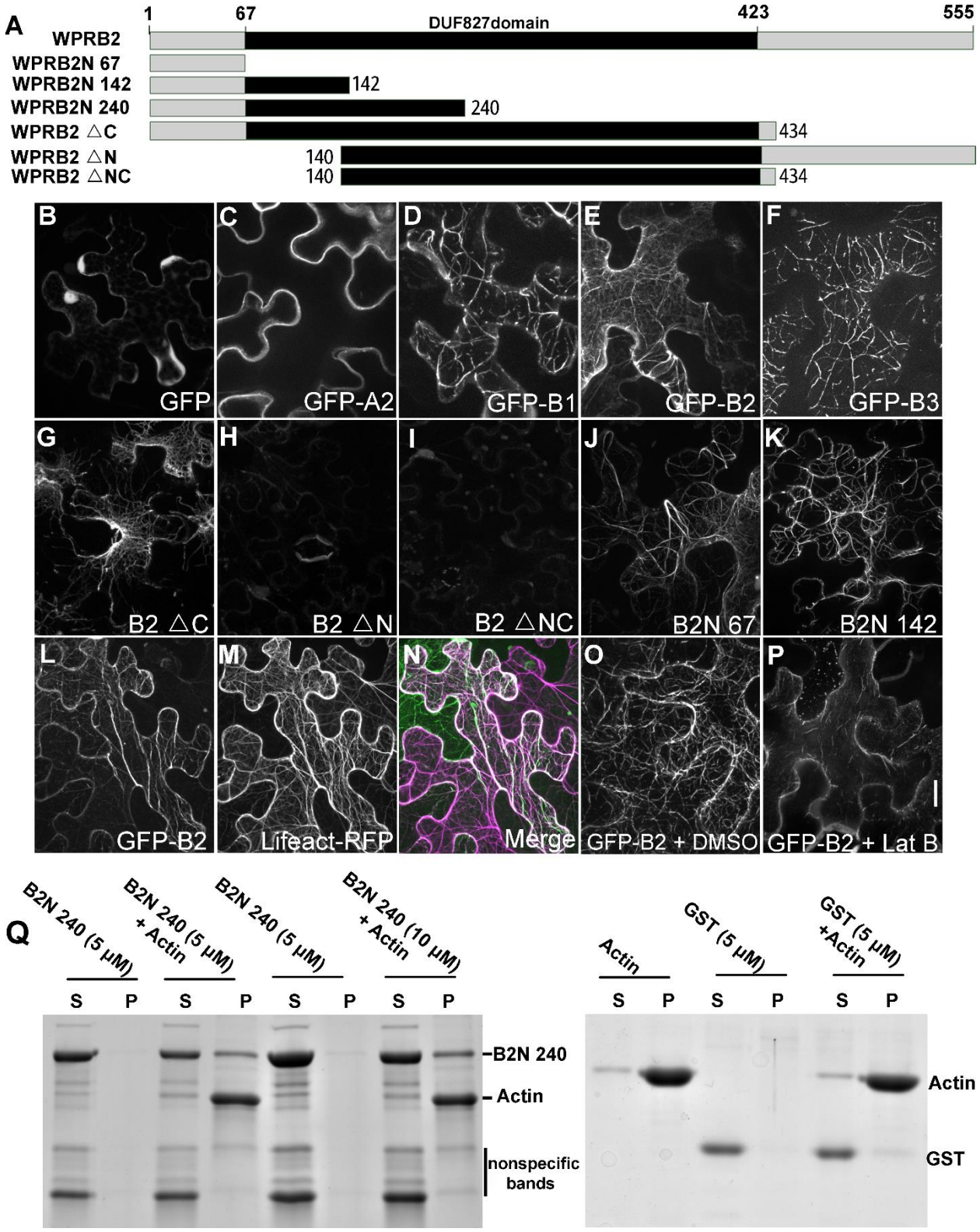


**Figure 6. WPRB interacts with F-actin. (A)** Schematic diagrams depicting WPRB2 and truncated versions. **(B-F)** Confocal images of transiently expressed full-length GFP fusion proteins in tobacco. Transient expression of GFP only **(B)**, GFP-WPRA2 **(C)**, GFP-WPRB1 **(D)**, GFP-WPRB2 **(E)** or GFP-WPRB3 **(F)**. **(G-K)** Transient expression of truncated WPRB2 proteins fused to GFP in tobacco leaves. Co-expression of GFP-WPRB2 **(L)** with Lifeact-RFP labeled actin microfilaments **(M)**; merged image **(N)** of the same cell. Tobacco leaves expressing GFP-WPRB2 were treated with DMSO **(**negative control, **O)** or 40 μM Latrunculin B **(P)** for 2 hours. All images at the same scale, Scale bar in **(P)** = 10 μm. **(Q)** High-speed co-sedimentation of GST-tagged WPRB2N240 with F-actin. After centrifugation at 100,000*g*, the proteins in the supernatant (S) and pellet (P) were resolved by SDS-PAGE and visualized with Coomassie Blue staining. GST protein was used as a negative control.

wanted to know if *wprb* mutants would enhance *pan2* phenotypes, similar to what has been observed in *rop2/4/9* mutants in combination with *pan1* (Humphries et al., 2011). However, we found that *wprb* mutations do not enhance the *pan2* phenotype (**Supplemental Figure 6**).

In addition to loss-of-function phenotypes, we examined our native promoter-fluorescent protein fusion transgenics to determine if mild overexpression, resulting from co-expression of these FPs in a wild type background with endogenous *Wpr* genes, would cause defective stomatal phenotypes. Plants expressing WPRB2-RFP or WPRA2-CFP in B73 indeed had mild subsidiary cell defects, further supporting that WPR proteins have a function in subsidiary cell division (**Figure 5 D, E**). These results indicate that both WPRA and WPRB family members participate in stomatal development, and suggest that WPRA1 and WPRA2 are important for the viability or function of male gametophytes.

**WPRB Proteins Directly Interact with F-actin**

Since WPR proteins contain no discernable domains other than DUF827, their molecular role is unclear. We hypothesized that WPRs might interact with F-actin, based on the importance of actin in SMC polarization, and because *A. thaliana* WEB1 and PMI2 have roles related to actin-based regulated chloroplast movement (Kodama et al., 2010). Although we did not see obvious co-localization of WPR proteins with actin filaments in maize, membrane localization has been observed for other known actin-associated proteins such as BRK1 and WAL (Facette et al., 2015; Sugiyama et al., 2019). When overexpressed in tobacco cells, WAL localizes to actin cables (as opposed to membranes). To determine whether overexpressed WPRs similarly co-localize with F-actin *in vivo*, we transiently overexpressed GFP-tagged WPRA2, WPRB1, WPRB2 and WPRB3 proteins in tobacco epidermal cells. GFP-WPRA2 localized at the cell periphery/membrane **(Figure 6C)**. However, GFP-WPRB1 **(Figure 6D)**, GFP-WPRB2 **(Figure 6E)** and GFP-WPRB3 **(Figure 6F)** were observed in filament-like structures. When GFP-WPRB2 is co-expressed with Lifeact-RFP (actin filament marker), the WPRB2-labeled filamentous structures extensively overlapped with Lifeact-RFP signals, particularly in the thick actin cables **(Figure 6L to 6N)**. We treated GFP-WPRB2 expressing tobacco leaves with Latrunculin B, an inhibitor of actin polymerization. The GFP-WPRB2 filamentous structures were disrupted, but remained intact in DMSO control **(Figure 6O and 6P)**. Thus, WPRB2 is an F-actin associated protein.

WPR proteins do not show significant sequence similarity to other known actin-associated proteins. To identify which region of the WPRB2 protein is responsible for its localization to filamentous structures, various WPRB2 fragments were used for transient tobacco expression assays **(Figure 6A)**. Surprisingly, the central conserved DUF827 domain is not responsible for filamentous localization. Instead, we found that the N-terminal 67 amino acids of WPRB2 is sufficient for filamentous localization in tobacco cells **(Figure 6J)**. Longer fragments containing the N-terminal 67 amino acids of WPRB2 were also found in filamentous structures, including GFP-WPRB2ΔC **(Figure 6G)** and GFP-WPRB2N142 **(Figure 6K)**. Any construct lacking the N-terminal domain does not label actin filaments, such as GFP-WPRB2ΔN **(Figure 6H)** and GFP-WPR B2ΔNC **(Figure 6I)**. We obtained similar results using full-length and truncated CFP-tagged constructs that were fused at C-terminus (rather than N-terminus) of WPRB2 **(Supplemental Figure 7)**. Conserved residues in the N-terminus of DUF827 proteins are highlighted in **Supplemental Figure 8.** Together, these data confirm that the N-terminal 67 amino acids of WPRB2 are necessary and sufficient for its filamentous localization.

To ask whether WPRB2 directly interacts with F-actin, we performed *in vitro* actin co-sedimentation assays. We used the slightly larger WPRB2N240 fragment, as the smaller WPRB2N67 fragment is similar in size

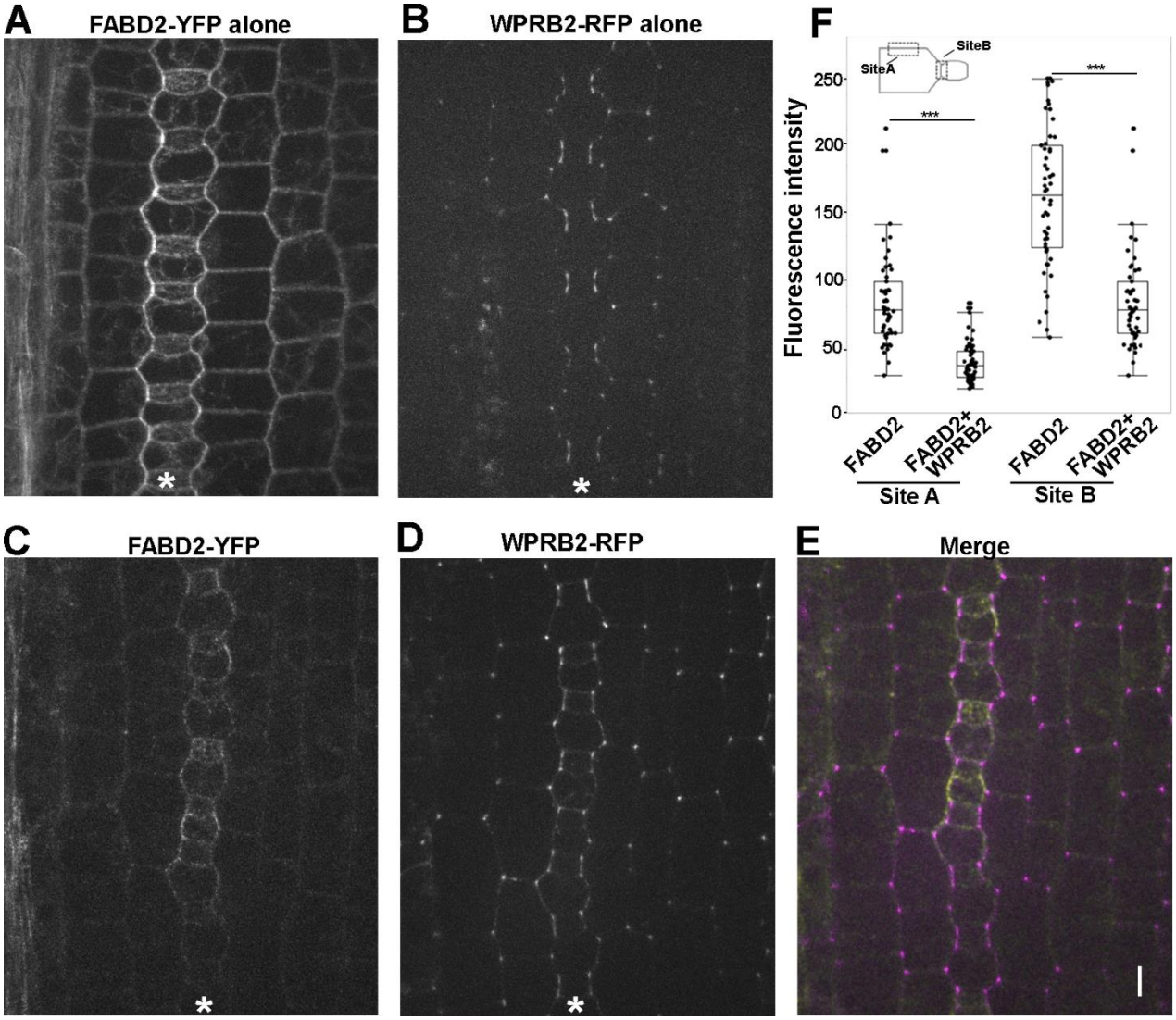


**Figure 7 The amount of F-actin decreases in WPRB2-RFP expressing plants.** Plants expressing WPRB2-RFP and FABD2-YFP were crossed, and the progeny independently segregated the two markers. **(A)** Plant only expressing FABD2-YFP. **(B)** Plant only expressing WPRB2-RFP. **(C-E)** Plant co-expressing FABD2-YFP (yellow in E) **(C)** with WPRB2-RFP (mageneta in E) and the merged image **(E).** **(F)** Quantification of fluorescence intensity of SMC lateral cell side (site A) and SMC-GMC interface (site B) in FABD2-YFP only plants (n = 4 plants, 108 cells) and WPRB2-RFP and FABD2-YFP co-expression plants (n = 3 plants, 102 cells). Two-way ANOVA test was performed. ***P < 0.0001. Scale bar = 5 µm.

to actin and made interpretation of the results difficult. WPRB2N240 is soluble in the absence of F-actin, but can be found in the pellet in the presence of F-actin **(Figure 6Q)**. The amount of WPRB2N240 appearing in the pellet is concentration dependent. Together, our localization and co-sedimentation experiments suggest that WPRB2 directly binds to F-actin via its N-terminal domain.

Physical interactions of WPR proteins with both PAN receptors and the actin cytoskeleton link together previously identified components of the BRK-PAN-ROP pathway. Potentially, WPRs may regulate actin polymerization, stability, or organization during some step of SMC polarization. Intriguingly, during co-localization experiments in stably transformed maize plants described earlier (**Figure 3**), we noticed that the fluorescence intensity of the actin marker FABD2-YFP was reduced in WPRB2-RFP co-expressing plants compared with RFP negative siblings, in all cell types. We

quantified the fluorescence, and found decreased FABD2-YFP fluorescence in SMCs at the GMC contact site as well as in adjacent pavement cells (**Figure 7**). This suggests that WPRB2 negatively affects the stability of filamentous actin.

Since actin is important in SMCs in early polarization, prior to WPR polarization (e.g., BRK proteins) and in late steps after WPR polarization (e.g. formation of the actin patch), we wanted to know if polarization of WPRB2 is maintained or stabilized by actin. We treated maize leaves expressing either WPRB2-RFP or FABD2-YFP with Latrunculin B. After 4 hours, 40 µm Latrunculin B treatment led to efficient depolymerization of actin in SMCs, including the dense patches of actin at the SMC-GMC interface **(Supplemental Figure 9)**. However, disruption of actin does not affect the localization of WPRB2-RFP. This suggests that WPRB2 is not dependent on actin networks for maintaining its polarization. Together, these results suggest that WPRB2 interacts with actin filaments in a manner that de-stabilizes them, at least when present in excess of normal amounts. This offers a potential explanation for how WPRs may impact actin-dependent processes in polarizing SMCs.

## DISCUSSION

We demonstrated that WPR proteins function in the BRK-PAN-ROP pathway for subsidiary cell formation during maize stomatal development, and physically interact with the receptor proteins PAN2 and PAN1. Like other proteins in the BRK-PAN-ROP pathway, WPRs polarize in SMCs at the site of GMC contact. The polarized accumulation of WPRs in SMC depends on PAN2, and genetic evidence demonstrates a function for WPRs in promoting normal SMC divisions. Like WEB1 and PMI2 in *A. thaliana*, different WPR subfamily members form heterodimers, suggesting WPR subfamily members co-operate to fulfill their function in different cellular contexts (Kodama et al., 2010).

Our analyses indicate that WPR proteins act downstream of PAN2, but upstream of PAN1, yet physically interact with both PAN1 and PAN2. This is the first observed physical link between PAN2 and PAN1, and offers a hypothesis of how PAN2 may promote polarization of PAN1, i.e. indirectly via WPR recruitment. We predict that in *wpr* mutants, PAN1 will no longer become polarized; however gene redundancy within the WPR family makes this a non-trivial question to address. Future experiments with high-order *wpr* mutants and PAN1-YFP will further elucidate the function of WPRs in the pathway the pathway. Even though WPRA2 and WPRB2 no longer polarize in *pan2* mutants, they still localize to the plasma membrane, indicating that membrane localization is independent of PAN2.

Our data indicate that both WPRA and WPRB proteins localize predominantly to the plasma membrane. Similar to the BRK1, which is important for acting regulation, WPR proteins also localize to cell corners (Facette et al., 2015). Previous studies using transient protoplast expression of WEB1 and PMI2 indicate WEB1 localizes to the plasma membrane, and can recruit PMI2 there (Kodoma et al., 2010). An independent proteomic study indicated that WEB1 is predominantly localized to the cytoplasm but re-localizes to the membrane (and its phosphorylation status changes) upon blue light irradiation (Deng et al., 2014). No DUF827 family members have predicted transmembrane domains, indicating their membrane association is either peripheral or via interactions with membrane-localized proteins, or perhaps via membrane-associated actin networks. Besides WEB1 and PMI2, the other characterized DUF827 protein is TREPH1 (Wang et al., 2018). TREPH1 and maize WPRA2 are orthologues **(Supplemental Figure 2)**. A specific residue in the C-terminus of TREPH1 is phosphorylated in response to touch, and the phenotype of the *treph1* mutant is dependent on the phosphorylation status of this residue (Wang et al., 2018). However, the

same residue in maize WPRA2 is not present. If all WPR proteins are similarly phosphoregulated, this suggests that other active, as of yet undiscovered kinases may be important for WPR regulation, since both PAN1 and PAN2 are pseudokinases.

Our analysis of CRISPR-Cas9 induced mutants of WPRs demonstrated that WPRs have diverse functions in maize. We were unable to recover *wpra1*/*wpra1*;*wpra2*/*wpra2* double mutants. WPRA1 and WPRA2 are 89% similar in protein sequence, and are highly expressed in pollen. WPRA2-CFP polarly localizes to the subapex of maize pollen tubes **(Supplemental Figure 5)**, raising the possibility that WPRA proteins play a role in pollen function. Additionally, we found *wprb1;wprb2* double mutants affect subsidiary cell formation, albeit not to the same extent as *pan* mutants. This may be caused by functional redundancy with other *Wpr* genes, such as *Wprb3*.

Our discovery that WPRB proteins directly bind actin is significant as it physically links them to actin network function. WPR proteins do not share any sequence homology to known actin binding proteins, however several DUF827 proteins were predicted, based on structural homology, to potentially bind the cytoskeleton (Gardiner et al., 2011). Surprisingly, the central conserved DUF827 domain is not the actin-binding domain. We mapped a 67 amino acid sequence that is necessary and sufficient for actin-binding, thereby identifying a putative novel actin binding domain. Within this sequence, there appears to be a motif that is conserved in many, but not all DUF827 proteins **(Supplemental Figure 8)**. Even though WPRA2 also contains most of this conserved domain, we did not observe co-localization of WPRA2 to the actin cytoskeleton. This could be because the transient expression does not reflect *in vivo* function. Alternatively, small differences between WPRA2 vs. B2 sequence may account for its lack of actin binding (e.g, one of a pair of glycines conserved in many WPR proteins is aspartate in WPRA2). Further refining the region of interaction, and determining if other DUF827 proteins bind actin, would inform their function.

The significance of WPR interaction with the actin cytoskeleton is unknown, and is complicated by the fact that there are several actin-related processes that occur during SMC polarization. The most plausible are: a function related to the SCAR/WAVE complex that includes BRK1, which polarizes and functions very early to promote SMC polarization; a role in localization of polarity determinants (such as vesicle trafficking); a role related to actin patch formation or function; or a role related to actin-based nuclear migration. These possibilities are not mutually exclusive. Actin filaments can facilitate polarized protein localization. For example, polarization of PIN requires an intact actin cytoskeleton (Kleine et al., 2008). It is plausible that actin networks are responsible for the polarization of PAN1 and/or PAN2, or even the WPR proteins themselves. This function would be distinct from that of the actin patch, which appears long after PAN2, PAN1, or WPR proteins polarize. When actin patches were disrupted with Latrunculin B, this did not result in the loss of already polarized WPRB2-RFP in maize leaves, suggesting the actin patch does not influence WPR protein localization (and possibly function). A clue to what WPR proteins could be doing *in vivo* can be inferred from our observation that WPRB2-RFP transgenic plants WPRB displayed less F-actin than controls. This suggests WPRB2 negatively affects the stability of actin filaments, and might promote F-actin depolymerization. Future *in vitro* and *in vivo* work characterizing the molecular role of WPR proteins on actin dynamics, including the nucleation, severing and bundling activities will help determine the function of this gene family – not only in cell polarization, but also during mechanosensing (i.e., TREPH1 function) or organelle movements (i.e. WEB1 and PMI2 function).

## METHODS

### Plant Materials and Plant Growth Condition

BRK1-CFP, PAN2-YFP, PAN1- YFP, and YFP-ABD2-YFP stable transgenic lines, and *brk1*, *pan1* and *pan2* mutants were described previously (Cartwright et al., 2009, Zhang et al., 2012; Facette et al., 2015). Plants used for analysis were grown for 10d to 14d in a greenhouse maintained between 20°C and 29°C with supplemental lighting (16-hour day length).

**Generation of transgenic maize lines**

Transgenic lines expressing WPRA2-CFP or WPRB2-RFP were created using a genomic construct. Primers are listed in **Supplemental Table 2.** An approximately 3kb sequence upstream of the start codon (promoter and 5' UTR) was amplified from B73 genomic DNA with primers WPRA2-F & WPRA2-P2 or WPRB2-F & WPRB2-P2. Genomic DNA, including all exons and introns 1kb after the stop codon (3' UTR), was amplified from B73 genomic DNA using primers WPRA2-P3 & WPRA2-R, or WPRB2-P3 & WPRB2-R. CFP or RFP was amplified with primer Tag linker-F and Tag linker-R as described previously (Mohanty et al., 2009). N-terminal fluorescent protein fusions were assembled through fusion PCR and cloned into pDONR221. Gateway LR reactions (Thermo Fisher) were used to recombine the assembled fusion protein into the binary vector pAM1006 (Monhanty et al., 2009). The constructions were verified and introduced into Hi-II maize via *Agrobacterium tumefaciens*–mediated transformation by Wisconsin Crop Innovation Center plant transformation facility. Primary transformants were crossed to B73 to produce T1 progeny used for immunoprecipitation experiments, and T1s were crossed with BRK1-CFP, PAN2-YFP, PAN1- YFP, and YFP-ABD2-YFP to produce T2 progeny used for the imaging experiments. Primary transformants were also crossed to *brk1*, *pan1* and *pan2* mutants, and the T1 progeny backcrossed again to mutants, to produce homozygous *brk1*, *pan1* and *pan2* mutants expressing WPRA2-CFP and WPRB2-RFP. In all cases, sibling plants grown simultaneously were used as controls.

**Yeast Two-Hybrid Analysis**

The GAL4-based yeast two-hybrid interaction system was used for interaction assays. The cDNA fragments encoding intracellular portions of PAN1 and PAN2 were cloned into pASGW-attR plasmid as a bait via Gateway cloning as described previously (Zhang et al., 2012). cDNA was prepared from the maize leaf stomatal division zone. Full length cDNAs of *Wpra1, Wpra2, Wprb1, Wprb2* and *Wprb3* cDNA were amplified from a maize leaf division zone cDNA preparation with primers WPRA1topo1-F + WPRA1topo-R (*Wpra1*), WPRA2topo1-F + WPRA2topo-R (*Wpra2*), WPRB1topo1-F + WPRB1topo-R(*Wprb1*) and WPRB2topo1-F + WPRB2topo-R (*Wprb2*) (**Supplemental Table 2**). These fragments were cloned into the entry vector pENTR/D-TOPO (Invitrogen) and further transferred destination vectors pASGW-attR (bait) and pACTGW-attR (prey) (Nakayama et al., 2002). Bait and prey plasmids were co-transformed into AH109 yeast strain. Yeast was grown on medium selecting for diploid cells (SD -Leu-Trp) or detecting interactions (SD -Leu-Trp-Ade-His) for two days at 30°C.

**Confocal Microscopy**

Plant tissues were observed using a custom-built spinning disc confocal unit (3i) equipped wih an inverted fluorescence microscope (IX83-ZDC, Olympus) CSU-W1 spinning disc with 50 micron pinholes (Yokogawa), aMesa Illumination Enhancement 7 Field Flattening unit (3i), an Andor iXon Life 888 EMCCD camera and a UPLANSAPO ×60 Silicone Oil-immersion objective (NA = 1.20, Olympus) and 4 laser stack with TTL controller (3i). For CFP, YFP and RFP imaging of transgenic maize plants, a 445/515/561 dichroic (Chroma) was used. All emission filters are from Semrock. A 445 nm laser line and 483/45 emission filter (CFP), 514 nm laser and 542/27 emission filter (YFP) or 568 laser with 618/50 emission filter (RFP) was used. For dual imaging of GFP and RFP (tobacco expression) a 405/488/561/640 dichoric (Chroma) was used, with a 488 nm

laser and 525/30 emission filter (GFP) and/or 568 laser with a 618/50 emission filter. Image processing was performed using Image Fiji and Adobe Photoshop version 8.0 using only linear adjustments and preserving hard edges.

**Transient expression in *N. benthamiana***

To generate 35S-expressed N-terminal GFP-tagged constructs (and truncated derivatives) and C-terminal CFP-tagged constructs (and truncated derivatives) for transient tobacco expression, coding sequence were PCR-amplified from maize leaf cDNA with the appropriate primers (**Supplementary Table 2**) and cloned into the pENTR/D-TOPO entry vector (Thermo Scientific). Clones were recombined with the vectors pSITE-2CA and pSITE-1NB using LR Clonase Mix II (Thermo Scientific) to form N-terminal GFP or C-terminal CFP (Romit Chakrabarty, 2006).

For transient expression in *N. benthamiana*, *Agrobacterium* strain GV3101 harboring different constructs were resuspended in infiltration buffer (10 mM MES (pH 5.7), 10 mM $MgCl_2$, 50 mg/L acetosyringone), and adjusted OD600 to 1.0. Equal volumes of cultures containing different constructs were mixed for co-infiltration. The resulting cultures were infiltrated into leaves of 3- to 4-week-old N. *benthamiana* plants. Leaf samples were harvested 48 hours after infiltration.

**Generation and Purification of WPRA1/A2 and WPRB2-Specific Antibody**

A peptide corresponding to amino acids 267 to 288 of maize WPRA1 and WPRA2 (LRNDFDPAAYDSLKEKLEQTNS) were synthesized, conjugated to KLH, co-injected into rabbits and used for polyclonal antibody production in rabbits by Pacific Immunology. And the resulting sera was affinity purified against the peptide using columns provided by Pacific Immunology. Affinity purifed antibodies were eluted using Gentle Ag/Ab buffer (Pierce), desalted against TBS Buffer, and concentrated to 1 mg/ml using a 30K MWCO concentrator (Pierce).

**Maize Division Zone Membrane Protein Extraction, Western Blotting, and Co-IP/MS Analysis**

Protein extraction for western blotting and co-IPs were performed as described previously (Facette et al., 2015). Briefly, 10-14 day old plants were used to isolate the basal 0.5-2.5 cm of unexpanded leaves 4-6, the leaf bases were ground in liquid nitrogen. Membrane fractions of extracts from these tissues were prepared. For western blotting, ~0.5 grams (3-5 plants) of tissue was used and for mass spectrometry, 1.5 grams (8-10 plants) were used. per 0.25 g of grounded tissue was mixed with 1ml extraction buffer (50mM Tris, pH 7.5, 150 mM NaCl, 5mM EGTA, 5mM EDTA 0.3% β-mercaptoethanol, 1% Sigma Plant Protease Inhibitor), the mixture was homogenized for 10s using an Omnitip homogenizer on ice. All subsequent steps were conducted at 4°C. The mixture was centrifuged twice at 13000*xg*. The supernatant was pelleted at 110,000xg for 45 min. Solubilization buffer (50 mM Tris pH 7.5, 150 mM NaCl, 1% NP-40, 10% glycerol, 0.05% Sodium deoxycholate) was then added to the pellet and following sonicated 3x15s and left rotating 1 hour. For western blotting, extracts from B73 plants and corresponded mutants were separated via SDS-PAGE and analyzed using anti-WPRA1/A2 at 1 µg/ml.

Co-IP/MS experiments were performed using the solubilized membrane proteins. Anti-WPRA1/A2 and anti-RFP were coupled with Dynabeads prepared according to the Dynabeads kit instructions (Thermo Fisher). The coupled WPRA1/A2 antibody-beads complex was added to the membrane protein extracts from B73 plants; uncoupled beads were used as a negative control. Anti-RFP coupled beads were added to the membrane protein extracts from WPRB2-RFP transgenic plants, and B73 plants as a negative control. All these samples were incubated rotating at room temperature for 30 min. Then the Dynabeads-

CO-IP complex was washed according to Dynabeads kit instructions. After washing, the Dynabeads-CO-IP complex was digested with trypsin and run with the mass spectrometer.

For Co-IP using anti-GFP to pull down WPRA2, anti-GFP beads (Miltenyi) were added to the extracts from WPRA2-CFP transgenic plants and B73 plants (negative control), then the extracts were rotated for an additional 30 minutes. Miltenyi µ columns were equilibrated using a solubilization buffer as described by instruction. The extracts were applied to the columns, the columns were washed and eluted as Miltenyi µ columns kit instruction, the eluted samples were digested with trypsin and run with the mass spectrometer.

**Genomic editing of maize WPRs by CRISPR–Cas9**

A dual gRNA maize CRISPR/Cas9 system was used to generate *Wpr* mutants (Char et al., 2017). Transgenic Hi-II maize plants were generated at the Iowa State Plant Transformation facility, expressing Cas9 from *Streptococcus pyogenes* under the maize UBI1 promotor and two guide RNAs under the rice U6.1 and U6.2 promotor, respectively. To create *wpra1* and *wpra2* mutants, two tandem gRNAs, gRNA1: GAAACATCTTTGGATATG and gRNA2: GTGCAAGCACACGAAGAAG were used to target identical sequences within *Wpra1* and *Wpra*2. To create *wprb1* and *wprb2* mutants, guide RNAs targeting *Wprb1* using gRNA1: GCTACATGTGATCTGGCTG or *Wprb2* using gRNA2: GCCTCCGTCGAGTCGCTG were used. Genomic edits were verified by Sanger sequencing of the target regions. Plants harboring edits were crossed to B73. Edited plants that no longer contain the transgene were confirmed and used for further analyses.

**Bacterial Expression of WPR proteins**

The DNA sequence of WPRB2N (1-240), which was used in the actin co-sedimentation assay, was amplified by PCR using the primers listed in Supplemental Table 2 and cloned into pGEX4T-1. Fragments of WPRA1 (63-503) WPRA2 (63-570) WPRB1 (73-421) and WPRB2 (78-429), which were used to confirm the specificity of the WPRA1/WPRA2 antibody, were also amplified by PCR using the primers listed in Supplemental Table 2 and cloned into pGEX4T-1 (Novagen) using BamHI/EcoRI sites to N-terminal glutathione S-transferase (GST) tag fusions. These constructions were transformed into *Escherichia coli* BL21 host strains (Novagen). GST fused proteins were induced with 0.5 mM isopropyl β-d-1-thiogalactopyranoside for 20 hours at 28°C. Affinity purified using glutathione-Sepharose 4B column (GE Healthcare) was carried out as described (Harper and Speicher, 2011).

**F-Actin Co-sedimentation Assay**

WPRB2N240 was dialyzed overnight against buffer A3 (10 mM Tris-HCl, 0.2 mM CaCl2, 0.2 mM ATP, and 0.5 mM DTT, PH=7.0 ). Prior to use, the protein was further purified by centrifugation at 100,000g for 1 hour at 4°C and only soluble protein was used for the assay. A high-speed co-sedimentation assay was performed as described previously (Xiang et al., 2007), Briefly, 5 µM and 10 µM WPRB2N240 alone or mixed with 4 µM preformed F-actin and incubated in 200 µL volume of buffer A3 for 1 hour at 25°C. The samples were centrifuged at 100,000g for 1 hour at 4°C. GST protein was used as a negative control. The supernatants and pellets were separated and subjected to SDS-PAGE and visualized by Coomassie Blue staining.

**Latrunculin B treatment**

To transiently depolymerize actin microfilaments in maize leaves, leaf 4 of two-week-old plants were excised and the basal 1 to 3 cm part was immersed in 40 µM Lat B (20 mM stock in DMSO) for 4 hours at room temperature. To examine the Latrunculin effect on the localization of GFP-WPRB2 in tobacco leaves, the GFP expressed tobacco leaves were cut into 0.5 cm×0.5 cm and covered with

40 µM Latrunculin B for 2 hours at room temperature.

**Gene tree construction**

Amino acid sequences of maize WPR homologs were identified using pBLAST against maize genomes. The gene tree was constructed in Molecular Evolutionary Genetics Analysis 11 (MEGA 11) software (Tamura et al., 2011) with the following parameters: multiple amino acids sequence alignment with ClustalW, phylogenetic construction with the maximum likelihood method, and bootstrap tests of 1,000 replicates. WPRs sequences used for the phylogenetic analysis are provided in **Supplementary File 1**.

**Accession Numbers**

Gene and protein sequences can be found at MaizeGDB www.maizegdb.org. Accession numbers for Version 4.0/Version 5.0 of the B73 genome are: *Wpra1:* Zm00001d023629/ Zm00001eb408590; *Wpra2*: Zm00001d041088/ Zm00001eb133280; *Wprb1:* Zm00001d0475516/ Zm00001eb395070; *Wprb2:* Zm00001d007164/ Zm00001eb111490; *Wprb3:* and Zm00001d010610/ Zm00001eb351980; *Brk1:* no v4.0/ Zm00001eb259430; *Pan2:* Zm00001d007862/ Zm00001eb117610; *Pan1*: Zm00001d031437/ Zm00001eb034900.

## ACKNOWLEDGEMENTS

We thank Steve Eyles at the UMass Institute of Applied Life Sciences Mass Spectrometry Facility. We thank Chris Phillips, Bob Skalbite, Neal Woodward, and other greenhouse and farm staff at the University of Massachusetts Amherst for essential help. This work was supported by a grant from the National Science Foundation (IOS-1754665) to MRF.

## AUTHOR CONTRIBUTIONS

M.F. and Q.N. designed and performed the research, analyzed the data and wrote the manuscript. S.N.C. and B.Y. designed the WPRs CRISPR sgRNAs and prepared the constructs for maize transformation.

## REFERENCES

**Apostolakos, B.G.P.** (2004). The role of the cytoskeleton in the morphogenesis and function of stomatal complexes. New Phytol. **161,** 613–639.

**Apostolakos, P., P. Livanos, E. Giannoutsou, E. Panteris, and Galatis B.** (2018) The intracellular and intercellular cross-talk during subsidiary cell formation in Zea mays: Existing and novel components orchestrating cell polarization and asymmetric division. Annals of Botany **122**, 679-696.

**Ashraf, M.A., and Facette, M.** (2020). Plant Biology: BASL Gives the Plant Nucleus a Sense of Direction. Curr. Biol. **30,** R1375-R1377.

**Campos, R., Goff, J., Rodriguez-Furlan, C., and Van Norman, J.M.** (2020). The Arabidopsis Receptor Kinase IRK Is Polarized and Represses Specific Cell Divisions in Roots. Dev. Cell **52,** 183-195.

**Cartwright, H.N., Humphries, J.A., and Smith, L.G.** (2009). PAN1: a receptor-like protein that promotes polarization of an asymmetric cell division in maize. Science **323,** 649-651.

**Char, S. N., Neelakandan, A. K., Nahampun, H., Frame, B., Main, M., Spalding, M. H., Becraft, P. W., Meyers, B. C., Walbot, V., Wang, K., & Yang, B.** (2017). An Agrobacterium-delivered CRISPR/Cas9 system for high-frequency targeted mutagenesis in maize. *Plant biotechnology journal*, *15*(2), 257–268. https://doi.org/10.1111/pbi.12611.

**Deng, Z., Oses-Prieto, J.A., Kutschera, U., Tseng, T.S., Hao, L., Burlingame, A.L., Wang, Z.Y., and Briggs, W.R.** (2014). Blue light-induced proteomic changes in etiolated Arabidopsis seedlings. J. Proteome Res. **13,** 2524-2533.

**De Smet I., and Beeckman T.** (2011). Asymmetric cell division in land plants and algae: the driving force for differentiation. Nat. Rev. Mol. Cell Biol. **12,** 177– 188.

**Dong, J., MacAlister, C.A., and Bergmann, D.C.** (2009). BASL controls asymmetric cell division in Arabidopsis. Cell **137,** 1320-1330.

**Facette, M.R., and Smith, L.G.** (2012). Division polarity in developing stomata. Curr. Plant Biol. **15,** 585-592.

**Facette M.R., Park Y., Sutimantanapi D., Luo A., Cartwright H., Yang, B., Bennett E.J., Sylvester A.W., and Smith L.G.** (2015). The SCAR/WAVE complex polarizes PAN receptors and promotes division asymmetry in maize. Nat. Plants **1,** 14024.

**Facette, M.R., Rasmussen, C.G., and Van Norman, J.M.** (2019). A plane choice: coordinating timing and orientation of cell division during plant development. Curr. Plant Biol. **47,** 47-55.

**Frank, M. J. and Smith, L. G.** (2002). A small, novel protein highly conserved in plants and animals promotes the polarized growth and division of maize leaf epidermal cells. Curr. Boil. **12,** 849-853.

**Galatis B., and Apostolakos P.** (2004). The role of the cytoskeleton in the morphogenesis and function of stomatal complexes. New Phytol. **161,** 613–639.

**Gardiner, J., Overall, R., and Marc, J.** (2011). Putative Arabidopsis homologues of metazoan coiled-coil cytoskeletal proteins. Cell Biol. Int. **35,** 767-774.

**Gray, A., Liu, L., and Facette, M.** (2020). Flanking Support: How Subsidiary Cells Contribute to Stomatal Form and Function. Front. Plant Sci. **11,** 881.

**Gu, Y., Fu, Y., Dowd, P., Li, S., Vernoud, V., Gilroy, S., and Yang, Z.** (2005). A Rho family GTPase controls actin dynamics and tip growth via two counteracting downstream pathways in pollen tubes. J. Cell Biol. **169,** 127-138.

**Hadley, R., Hable, W.E., and Kropf, D.L.** (2006). Polarization of the endomembrane system is an early event in fucoid zygote development. BMC Plant Boil. **6,** 5.

**Harper S, Speicher DW.** (2011) Purification of proteins fused to glutathione S-transferase. Methods Mol Biol. **681,** 259–80.

**Houbaert, A., Zhang, C., Tiwari, M., Wang, K., de Marcos Serrano, A., Savatin, D.V., Urs, M.J., Zhiponova, M.K., Gudesblat, G.E., Vanhoutte, I., Eeckhout, D., Boeren, S., Karimi, M., Betti, C., Jacobs, T., Fenoll, C., Mena, M., de Vries, S., De Jaeger, G., and Russinova, E.** (2018). POLAR-guided signalling complex assembly and localization drive asymmetric cell division. Nature **563,** 574-578.

**Humphries, J.A., Vejlupkova, Z., Luo, A., Meeley, R.B., Sylvester, A.W., Fowler, J.E., and Smith, L.G. (2011).** ROP GTPases act with the receptor- like protein PAN1 to polarize asymmetric cell division in maize. Plant cell **23,** 2273-2284.

**Kennard J. L., Cleary A. L.** (1997). Pre-Mitotic Nuclear Migration in Subsidiary Mother Cells of Occurs in G1 of the Cell Cycle and Requires F-Actin. Cell Motil. Cytoskelet. **36,** 55-67.

**Kleine-Vehn, J., Langowski, L., Wisniewska, J., Dhonukshe, P., Brewer, P.B., and Friml, J.** (2008). Cellular and molecular requirements for polar PIN targeting and transcytosis in plants. Mol. plant **1,** 1056-1066.

**Kimata, Y., Higaki, T., Kawashima, T., Kurihara, D., Sato, Y., Yamada, T., Hasezawa, S., Berger, F., Higashiyama, T., and Ueda, M.** (2016). Cytoskeleton dynamics control the first asymmetric cell division in Arabidopsis zygote. Proc Natl Acad Sci USA **113,** 14157-14162.

**Kodama, Y., Suetsugu, N., and Wada, M.** (2011). Novel protein-protein interaction family proteins involved in chloroplast movement response. Plant Signal. Behav. **6,** 483-490.

**Kodama, Y., Suetsugu, N., Kong, S.G., and Wada, M.** (2010). Two interacting coiled-coil proteins, WEB1 and PMI2, maintain the chloroplast photorelocation movement velocity in Arabidopsis. Proc. Natl. Acad. Sci. USA **107,** 19591-19596.

**Larkin, M.A., Blackshields, G., Brown, N.P., Chenna, R., McGettigan, P.A., McWilliam, H., Valentin F., Wallace, I.M., Wilm A., Lopez, R., Thompson, J.D., and Gibson, T.J.** (2007) Clustal W and Clustal X version 2.0. Bioinformatics, **23,** 2947–2948.

**Lau, O.S., and Bergmann, D.C.** (2012). Stomatal development: a plant's perspective on cell polarity, cell fate transitions and intercellular communication. Development **139,** 3683-3692.

**Lee JS, Kuroha T, Hnilova M, Khatayevich D, Kanaoka MM, McAbee JM, Sarikaya M, Tamerler C, Torii KU.** (2012). Direct interaction of ligand–receptor pairs specifying stomatal patterning. *Genes Dev* **26,** 126–136.

**Lipka, E., Herrmann, A., and Mueller, S.** (2015). Mechanisms of plant cell division. Wiley interdisciplinary reviews. Dev. Biol. **4,** 391-405.

**Luesse, D.R., DeBlasio, S.L., and Hangarter, R.P.** (2006). Plastid movement impaired 2, a new gene involved in normal blue-light-induced chloroplast movements in Arabidopsis. Plant Physiol. **141,** 1328-1337.

**Mohanty, A., Luo, A., DeBlasio, S., Ling, X., Yang, Y., Tuthill, D.E., Williams, K.E., Hill, D., Zadrozny, T., Chan, A., Sylvester, A.W., and Jackson, D.** (2009). Advancing cell biology and functional genomics in maize using fluorescent protein-tagged lines. Plant Physiol. **149,** 601-605.

**Muroyama, A., Gong, Y., and Bergmann, D.C.** (2020). Opposing, Polarity-Driven Nuclear Migrations Underpin Asymmetric Divisions to Pattern Arabidopsis Stomata. Curr. Biol. **30,** 4467-4475

**Nakayama M., Kikuno R., Ohara O.** (2002). Protein-protein interactions between large proteins: Two-hybrid screening using a functionally classified library composed of long cDNAs. Genome Res. **12,** 1773–1784.

**Nunes, T.D.G., D. Zhang, and M.T. Raissig.** (2020). Form, development and function of grass stomata. Plant J. **101,** 780-799

**Pillitteri, L.J., Peterson, K.M., Horst, R.J., and Torii, K.U.** (2011). Molecular profiling of stomatal meristemoids reveals new component of asymmetric cell division and commonalities among stem cell populations in Arabidopsis. Plant Cell **23,** 3260 – 3275.

**Pillitteri, L.J., and Torii, K.U. (2012).** Mechanisms of stomatal development. Annu. Rev. Plant Biol. **63,** 591 – 614.

**Romit Chakrabarty, R.B., Sang-Min Chung, Mark Farman, Vitaly Citovsky, Saskia A. Hogenhout, Tzvi Tzfira, and Michael Goodin** (2006). pSITE Vectors for Stable Integration or Transient Expression of Autofluorescent Protein Fusions in Plants: Probing Nicotiana benthamiana–Virus Interactions Plant Physiol. **20,** 740–750.

**Raissig MT, Matos JL, Anleu Gil MX, Kornfeld A, Bettadapur A, Abrash E, Allison HR, Badgley G, Vogel JP, Berry JA, Bergmann DC.** (2017). Mobile MUTE specifies subsidiary cells to build physiologically improved grass stomata. Science **355,** 1215–1218.

**Shao, W., and Dong, J.** (2016). Polarity in plant asymmetric cell division: Division orientation and cell fate differentiation. Dev. Biol. **419,** 121-131.

**Sugiyama, Y., Nagashima, Y., Wakazaki, M., Sato, M., Toyooka, K., Fukuda, H., and Oda, Y.** (2019). A Rho-actin signaling pathway shapes cell wall boundaries in Arabidopsis xylem vessels. Nat. Commun. **10,** 468.

**Sutimantanapi, D., Pater, D., and Smith, L.G.** (2014). Divergent roles for maize PAN1 and PAN2 receptor-like proteins in cytokinesis and cell morphogenesis. Plant Physiol. **164,** 1905-1917.

**Stebbins, G.L., and Shah, S.S.** (1960). Developmental studies of celldifferentiation in the epidermis of monocotyledons. II. Cytological features of stomatal development in the Gramineae. Dev. Biol. **2,** 477 – 500.

**Tamura K. Peterson D. Peterson N. Stecher G. Nei M. Kumar S.** (2011). MEGA5: Molecular evolutionary genetics analysis using maximum likelihood, evolutionary distance, and maximum parsimony methods. Mol. Biol. Evol. **28,** 2731–2739.

**Walley, J.W., Sartor, R.C., Shen, Z., Schmitz, R.J., Wu, K.J., Urich, M.A., Nery, J.R., Smith, L.G., Schnable, J.C., Ecker, J.R., and Briggs, S.P.** (2016). Integration of omic networks in a developmental atlas of maize. Science. **353,** 814-818

**Wang, K., Yang, Z., Qing, D., Ren, F., Liu, S., Zheng, Q., Liu, J., Zhang, W., Dai, C., Wu, M., Chehab, E.W., Braam, J., and Li, N.** (2018). Quantitative and functional posttranslational modification proteomics reveals that TREPH1 plays a role in plant touch-delayed bolting. Proc. Natl. Acad. Sci. USA **115,** E10265-E10274.

**Wu, S.Z., and Bezanilla, M.** (2018). Actin and microtubule cross talk mediates persistent polarized growth. J. Cell Biol. **217,** 3531-3544.

**Xiang, Y., Huang, X., Wang, T., Zhang, Y., Liu, Q., Hussey, P.J., and Ren, H.** (2007). ACTIN BINDING PROTEIN 29 from Lilium pollen plays an important role in dynamic actin remodeling. Plant cell **19,** 1930-1946.

**Yang, Z.** (2008). Cell polarity signaling in Arabidopsis. Annu. Rev. Cell Dev. Biol. **24,** 551-575.

**Yoshida, S., van der Schuren, A., van Dop, M., van Galen, L., Saiga, S., Adibi, M., Moller, B., Ten Hove, C.A., Marhavy, P., Smith, R., Friml, J., and Weijers, D.** (2019). A SOSEKI-based coordinate system interprets global polarity cues in Arabidopsis. Nat. Plants **5,** 160-166.

**Zhang, X., Facette, M., Humphries, J.A., Shen, Z., Park, Y., Sutimantanapi, D., Sylvester, A.W., Briggs, S.P., and Smith, L.G.** (2012). Identification of PAN2 by quantitative proteomics as a leucine-rich repeat-receptor-like kinase acting upstream of PAN1 to polarize cell division in maize. Plant cell **24,** 4577-4589

| | Gene ID | Gene name | Rep1 # Unique Peptides | Rep2 # Unique Peptides | Rep3 # Unique Peptides | Control 1 # Unique Peptides | Control 2 # Unique Peptides | Control 3 # Unique Peptides |
|---|---|---|---|---|---|---|---|---|
| Anti-GFP | Zm00001d041088 | **WPRA2 (bait)** | 28 | 42 | 2 | 2 | 0 | 0 |
| | Zm00001d007164 | WPRB2 | 5 | 3 | 0 | 0 | 0 | 0 |
| | Zm00001d010610 | WPRB3 | 15 | 13 | 0 | 0 | 0 | 1 |
| | Zm00001d029420 | WEB subfamily protein | 5 | 7 | 0 | 0 | 0 | 0 |
| Anti-WPRA1/A2 | Zm00001d023629 | **WPRA1 (bait)** | 24 | 19 | 26 | 0 | 1 | 2 |
| | Zm00001d041088 | **WPRA2 (bait)** | 26 | 19 | 27 | 0 | 0 | 0 |
| | Zm00001d047516 | WPRB1 | 5 | 4 | 6 | 0 | 0 | 0 |
| | Zm00001d007164 | WPRB2 | 19 | 21 | 21 | 0 | 0 | 0 |
| | Zm00001d010610 | WPRB3 | 24 | 21 | 24 | 0 | 1 | 0 |
| | Zm00001d026193 | WPRC subfamily protein | 2 | 1 | 0 | 0 | 0 | 0 |
| | Zm00001d000443 | WPRC subfamily protein | 2 | 2 | 0 | 0 | 0 | 1 |
| | Zm00001d048523 | WEB subfamily protein | 2 | 2 | 2 | 0 | 0 | 0 |
| | Zm00001d007862 | PAN2 | 4 | 5 | 4 | 0 | 0 | 2 |
| | Zm00001d031437 | PAN1 | 2 | 5 | 2 | 0 | 0 | 0 |
| Anti-RFP | Zm00001d007164 | **WPRB2 (bait)** | 18 | 20 | 17 | 0 | 1 | 0 |
| | Zm00001d023629 | WPRA1 | 15 | 16 | 16 | 0 | 0 | 0 |
| | Zm00001d041088 | WPRA2 | 18 | 21 | 20 | 0 | 2 | 0 |
| | Zm00001d010610 | WPRB3 | 1 | 2 | 1 | 0 | 0 | 0 |
| | Zm00001d007862 | PAN2 | 3 | 0 | 1 | 0 | 0 | 0 |

**Table 1**. **WPR proteins interact with other WPR family members and PAN receptors.** WPR-interacting proteins identified by Co-IP/MS. For a complete list of all proteins, see Supplementary Data Set 1. Three different experiments were performed. 1: Anti-GFP was used to pull down WPRA2 and interacting proteins from extracts of plants expressing WPRA2-CFP, and from non-transgenic plants as a negative control. 2: Anti-WPRA1/A2 was used to pull down WPRA1/A2 and interacting proteins from B73 extracts; negative controls used the same extracts but omitted the anti-WPRA1/A2 antibody. 3: Anti-RFP was used to pull down WPRB2 and interactors from extracts of plants expressing WPRB2-RFP, and from non-transgenic plants as a negative control. B73 vs4 gene codes are used to identify proteins, and the number of unique peptides (# peptides) is listed. The baits WPRA2, WPRA1/A2, and WPRB2 are highlighted in bold.

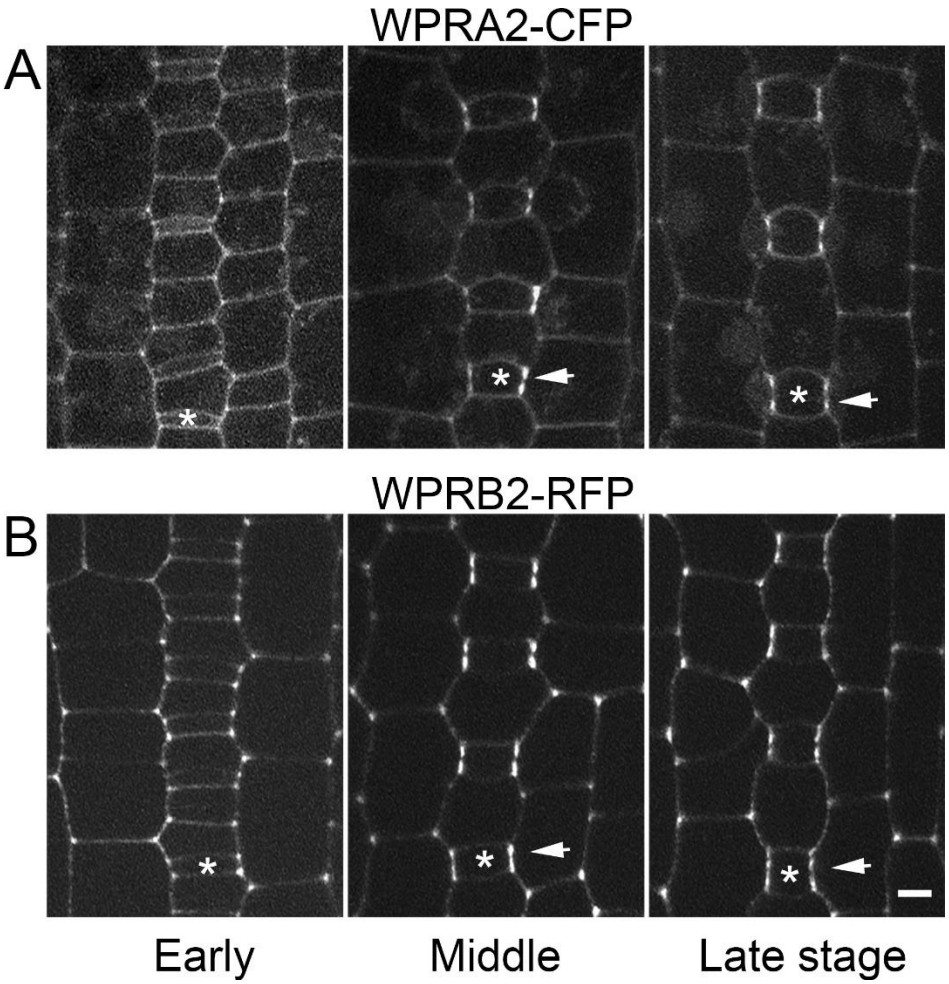


**Figure 1. WPRA2-CFP and WPRB2-RFP polarize in developing subsidiary mother cells.** The stomatal division zone of the fourth leaf of transgenic maize plants was dissected and analyzed. Three different stomatal development stages were selected according to GMC width and SMC division status to observe the localization of WPRA2-CFP (A) and WPRB2-RFP (B). Arrows point to sites of WPRA2-CFP or WPRB2-RFP accumulation in SMCs where they contact the adjacent GMC. Asterisks mark a GMC within each stomatal row. Scale bar = 5 µm.

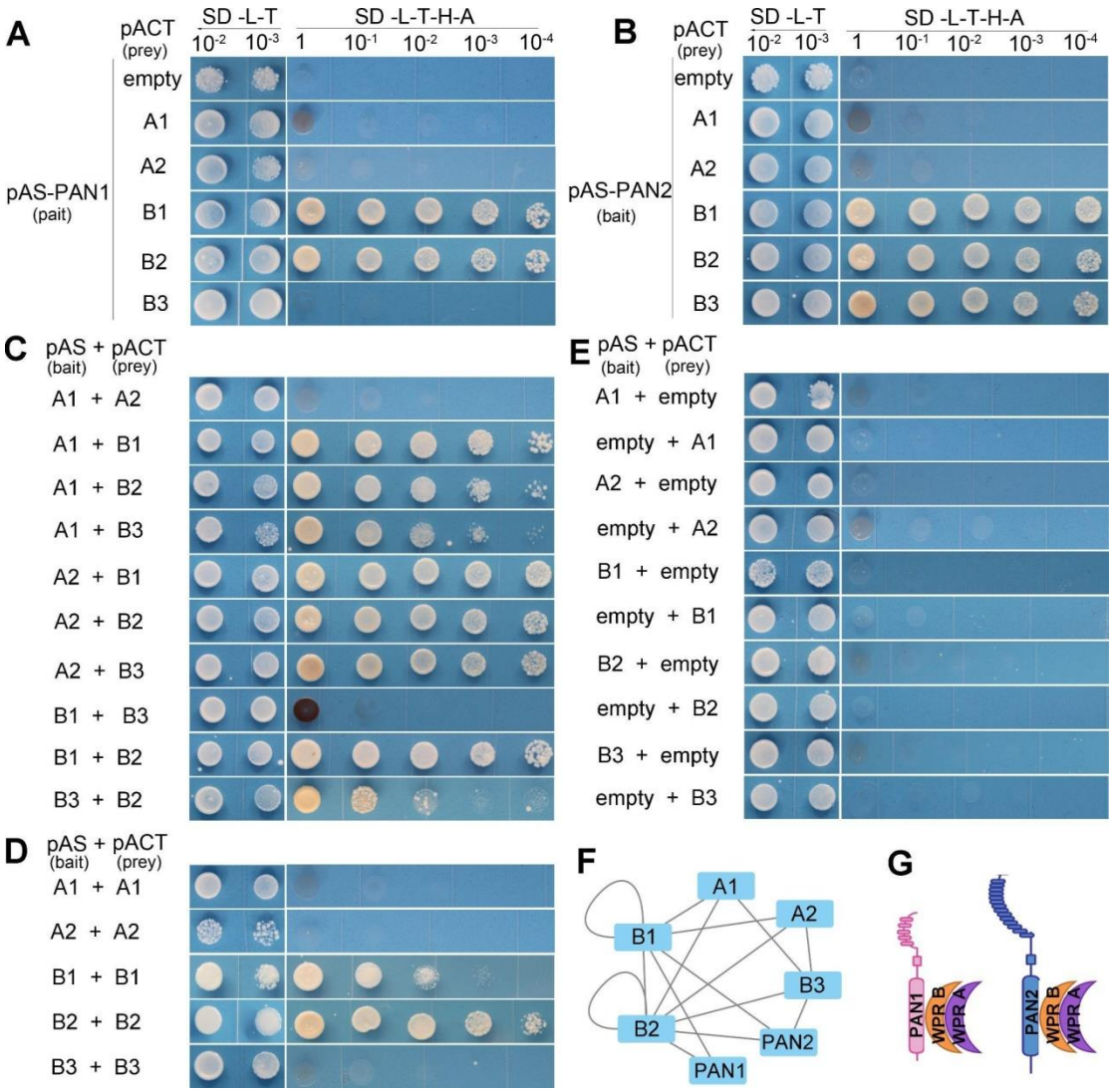


**Figure 2. Yeast 2-hybrid analysis of WPR and PAN protein interactions.** Interactions were assessed using the GAL4-based yeast two-hybrid system. Yeast was grown at different dilutions on non-selective (-L-T) and selective (-L-T-A-H) media. Soluble intracellular regions of PAN1 and PAN2 were used. **(A)** and **(B)**, interactions of PAN1 and PAN2 with WPRA1, WPRA2, WPRB1, WPRB2, and WPRB3. **(C)** Heterodimer formation was assessed between WPRA1, WPRA2, WPRB1, WPRB2, and WPRB3. **(D)** Homodimer formation was assessed between WPRA1, WPRA2, WPRB1, WPRB2, and WPRB3. **(E)** Negative controls using empty bait plasmid pASGW-attR or prey plasmid pACTGW-attR. **(F)** Network diagram showing the observed interactions between WPRs and PAN1/PAN2. **(G)** A model of protein complex formation between PAN and WPR proteins.

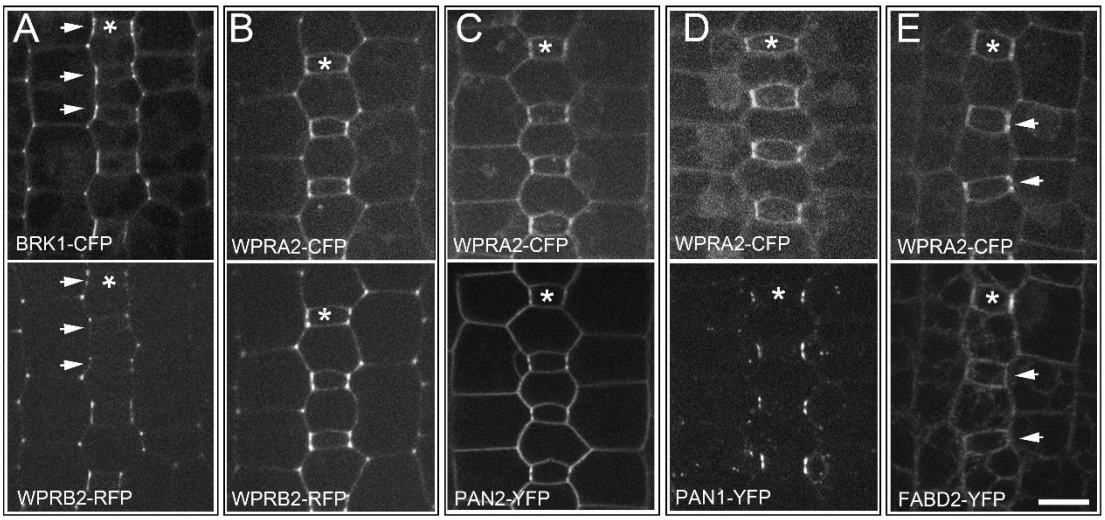


**Figure 3. WPR proteins polarize in SMCs after BRK1 and before actin.**
Plants co-expressing BRK1-CFP & WPRB2-RFP **(A)**, WPRA2-CFP & WPRB2-RFP **(B)**, WPRA2-CFP & PAN1-YFP **(C)**, WPRA2-CFP & PAN2-YFP **(D)**, or WPRA2-CFP and FABD2-YFP **(E)** were analyzed during stomatal development. Top and bottom panels are the same cells, imaged on different channels. Asterisks mark the top GMC in each panel. Fluorescent proteins were scored as polarized when fluorescence was brighter at the SMC-GMC interface than adjacent portions of the cell periphery. Arrows in **(A)** mark examples of cells in which BRK1-CFP is polarized, but not WPRB2-RFP. Arrows in **(E)** marker examples of cells in which WPRA2-CFP is polarized but not FABD2-YFP. Quantification of co-expression is in **Supplemental Table 1.** Scale bar = 10 µm.

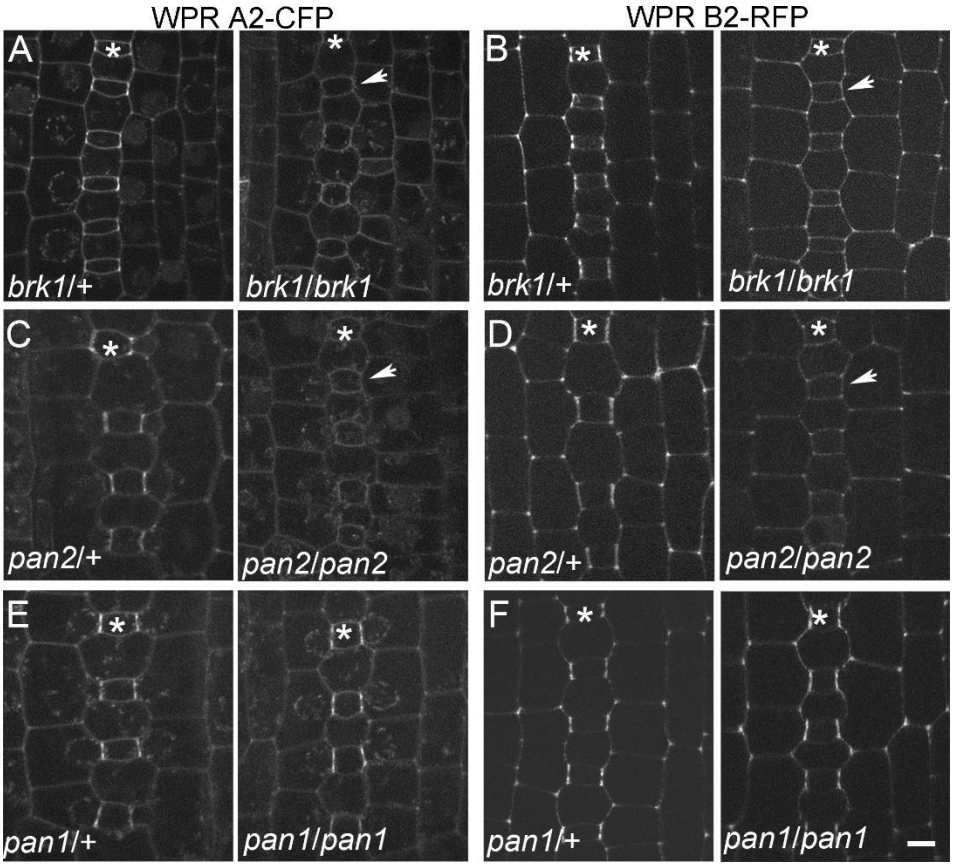


**Figure 4**. **Polarization of WPR proteins depends on BRK1 and PAN2, but not PAN1.**
Localization of WPRA2-CFP and WPRB2-RFP in *brk1*, *pan2* and *pan1* mutants and non-mutant siblings was analyzed in developing leaf 4.
WPRA2-CFP **(A)** and WPRB2-RFP **(B)** in developing stomata of *brk1* mutants and non-mutant (heterozygous) siblings. WPRA2-CFP **(C)** and WPRB2-RFP **(D)** in developing stomata of *pan2* mutants and non-mutant (heterozygous) siblings. WPRA2-CFP **(E)** and WPRB2-RFP **(F)** in developing stomata of *pan1* mutants and non-mutant (heterozygous) siblings. Asterisks mark GMC rows. Arrows point to SMCs without polarized localization of WPRA2-CFP or WPRB2-RFP. 3-6 plants of each genotype were used for data collection. Scale bar, 5 µm.

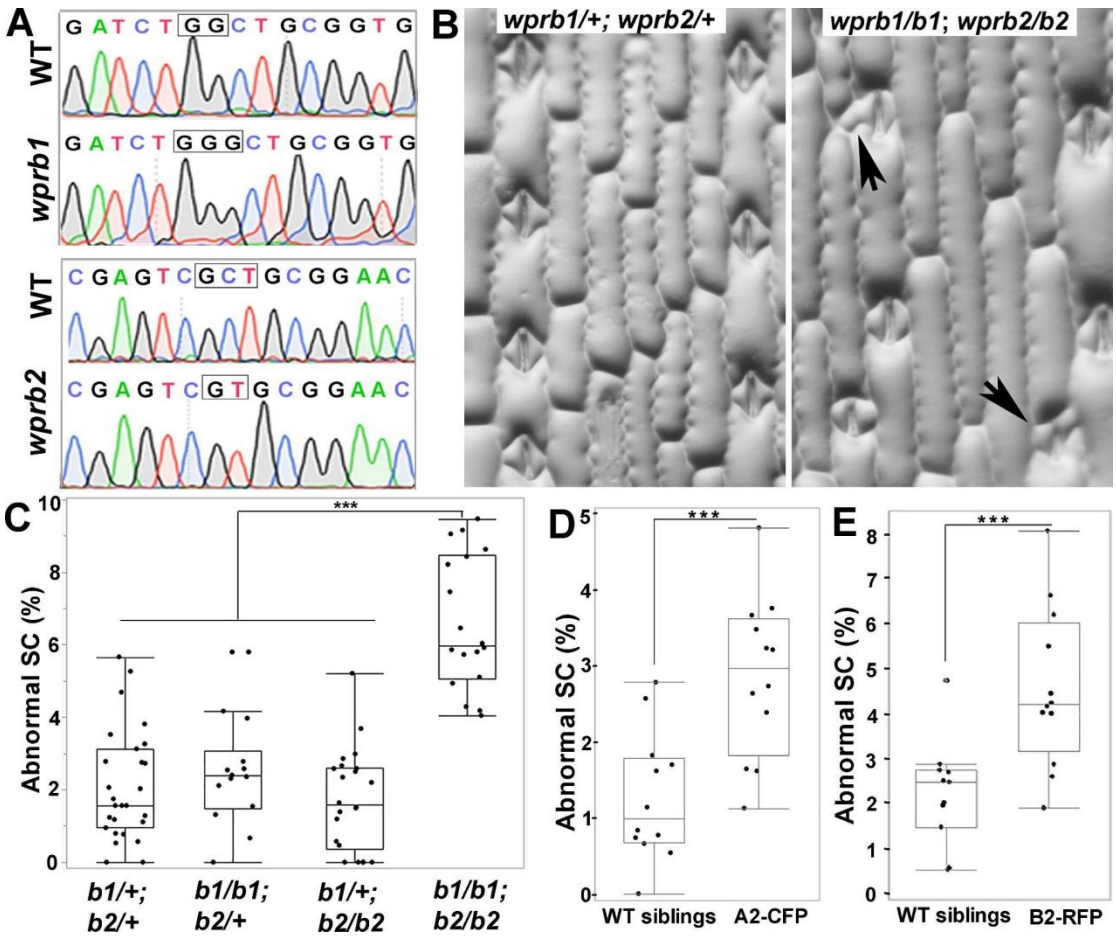


**Figure 5. CRISPR-Cas9 induced *wprb1*;*wprb2* double mutants and WPRA2-CFP and WPRB2-RFP overexpression lines have SC defects.**

**(A)** Cas9-edited *Wprb1* and *Wprb2* genes. Mutated regions are labeled in black square; *wprb1* has a "G" insertion and *wprb2* has a "C" deletion in the gRNA targeted region. These mutations cause frameshifts and premature termination. **(B)** Representative image of the third leaf epidermis of *wprb1*/+; *wprb2*/+ and *wprb1*/*wprb1*; *wprb2*/*wprb2* mutants. Black arrows indicate abnormal subsidiary cells. **(C)** Quantification of abnormal subsidiary cells (SC) in *wprb1*/+; *wprb2*/+ (n = 27 plants), *wprb1*/*b1*;*wprb2*/+ (n = 14 plants), *wprb1*/+;*wprb2*/*wprb2* (n = 22 plants) and *wprb1*/*wprb1*;*wprb2*/*wprb2* (n=18 plants). For each plant 100-200 subsidiary cells were examined. p-value from Student's T-test comparing each genotypes, ***P≤ 0.001. **(D)** and **(E)** Quantification of abnormal subsidiary cells in WPRA2-CFP or WPRB2-RFP expressing plants and non-transgenic siblings grown in parallel. (n = 11-12 plants and about 120-200 cells per genotype). Student's T-test were performed, ***p≤ 0.001.

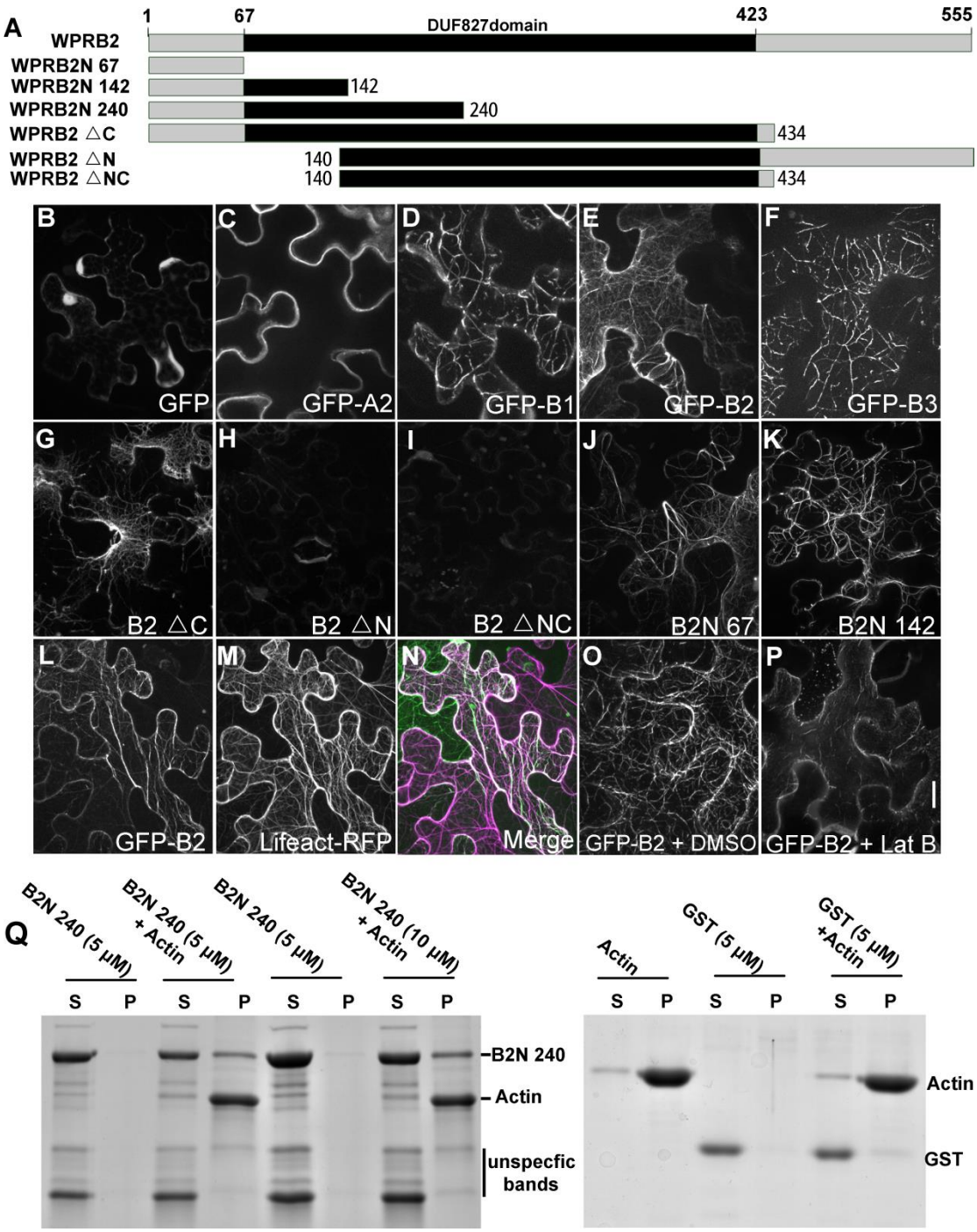


**Figure 6. WPRB interacts with F-actin.**

**(A)** Schematic diagrams depicting WPRB2 truncated versions fused with N-terminal GFP as shown in (G-K). **(B-F)** Confocal images of full-length transiently-expressed fluorescent proteins in tobacco. Transient expression of GFP only **(B)**, GFP-WPRA2 **(C)**, GFP-WPRB1 **(D)**, GFP-WPRB2 **(E)** or GFP-WPRB3 **(F)**. **(G-K)** Transient expression of truncated WPRB proteins fused to GFP in tobacco leaves. Co-expression of GFP-WPRB2 **(L)** with Lifeact-RFP labeled actin microfilaments **(M)**; merged image **(N)** of the same cell. Tobacco leaves expressing GFP-WPRB2 were treated with DMSO **(**negative control, **O)** or 40 μM Latrunculin B **(P)** for 2 hours. All images at the same scale, Scale bar in **(P)** = 10 μm. **(Q)** High-speed co-sedimentation of GST-tagged WPRB2N240 with F-actin. After centrifugation at 100,000*g*, the proteins in the supernatant (S) and pellet (P) were

resolved by SDS-PAGE and visualized with Coomassie Blue staining (?). GST protein was used as a negative control.

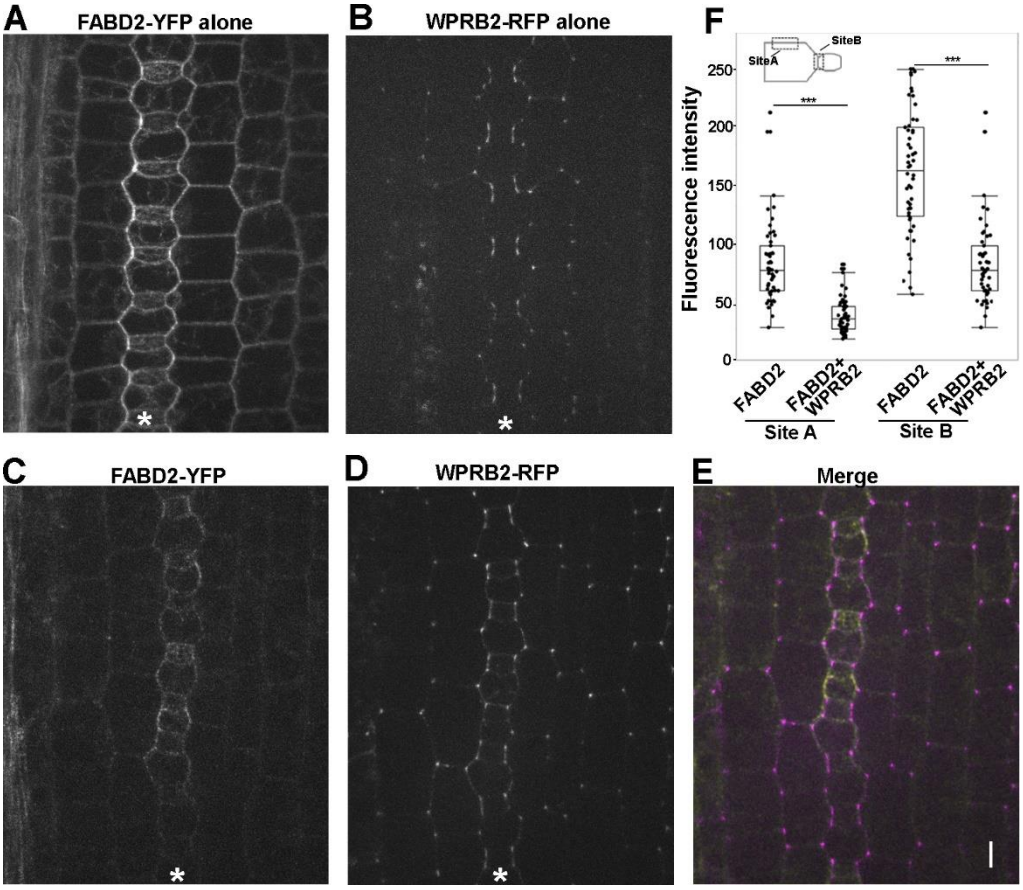


**Figure 7 The amount of F-actin decreases in WPRB2-RFP overexpression plants.** Plants expressing WPRB2-RFP and FABD2-YFP were crossed, and the progeny independently segregated the two markers. **(A)** Plant only expressing FABD2-YFP. **(B)** Plant only expressing WPRB2-RFP. **(C-E)** Plant co-expressing FABD2-YFP(yellow in E) **(C)** with WPRB2-RFP (mageneta in E) and the merged image **(E).** **(F)** Quantification of fluorescence intensity of SMC lateral cell side (site A) and SMC-GMC interface (site B) in FABD2-YFP only plants (n = 4 plants, 108 cells) and WPRB2-RFP and FABD2-YFP co-expression plants (n = 3 plants, 102 cells). Two-way ANOVA test was performed. ***P < 0.0001. Scale bar = 5 µm.

## SUPPLEMENTAL DATA

**Supplemental Figure 1. Maize stomatal development.**

**Supplemental Figure 2. Phylogenetic relationships between *A. thaliana* and *Z. mays* WPR proteins**

**Supplemental Figure 3. Plasmolysis assays of WPRA2-CFP and WPRB2-RFP transgenic plants.**

**Supplemental Figure 4. Validation of anti-WPRA1/A2 antibody**

**Supplemental Figure 5. CRISPR-Cas9 induced *Wpra1 and Wpra2* mutants might have transmission defects.**

**Supplemental Figure 6. Knockout of *Wprb1* and *Wprb2* do not enhance *pan2*/*pan2* mutant's phenotype.**

**Supplemental Figure 7. Transient expression of WPRB2-CFP, and its truncated proteins in tobacco leaves.**

**Supplemental Figure 8. Alignment of the actin-binding domain of the WPR protein family.**

**Supplemental Figure 9. F-actin disruption does not affect the polarized localization of WPRB2-RFP in SMCs.**

**Supplemental Table 1. Co-expression of polarized fluorescent protein markes in SMCs.**

**Supplemental Table 2. Primer sequences used in this study.**

**Supplemental Data Set 1. List of WPRA and WPRB interactors identified by Co-IP/MS.**

**Supplemental File 1. Amino acid sequences of WPRs used for the phylogenetic analysis in Supplemental Figure 2.**

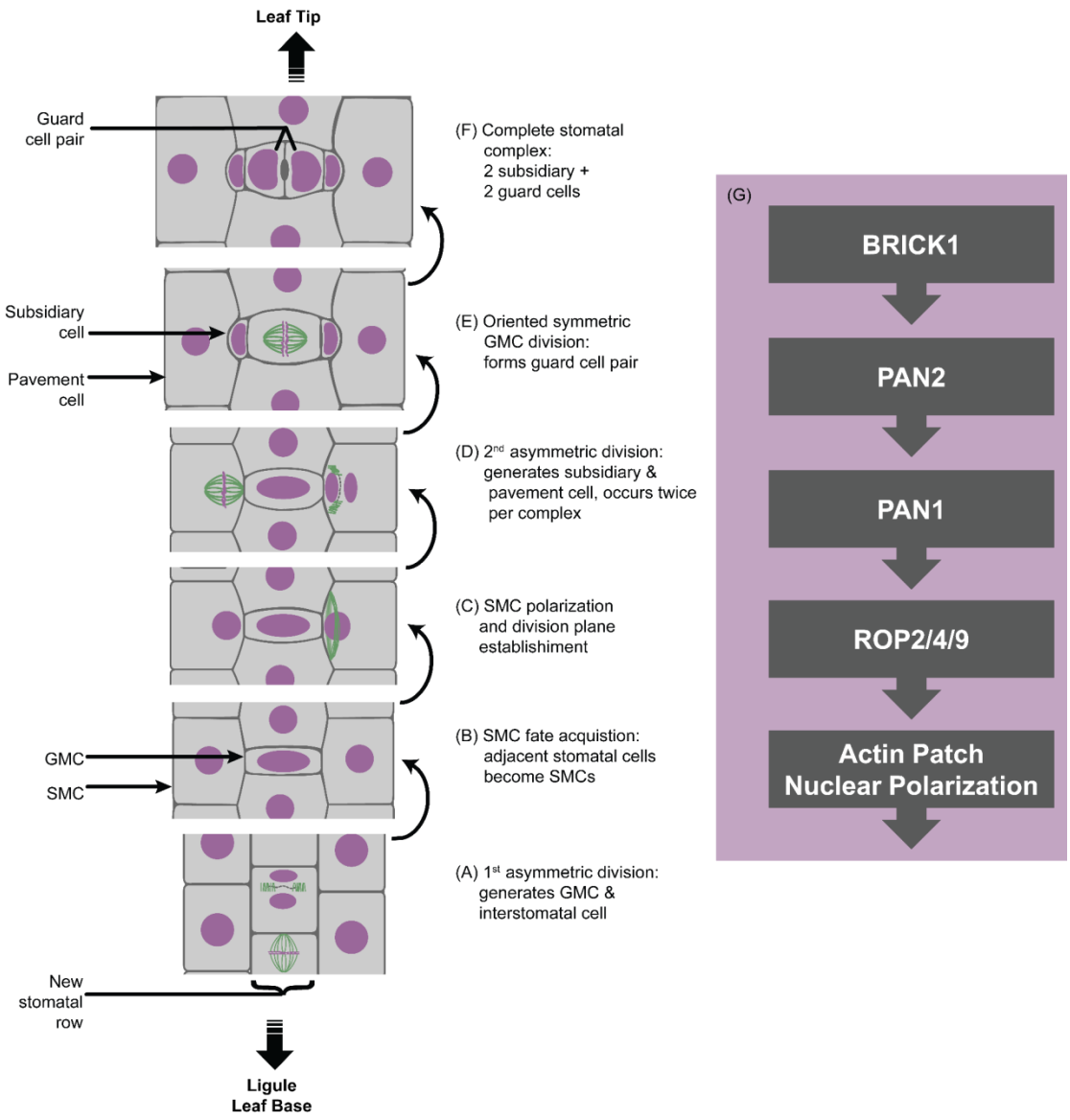


**Supplemental Figure 1. Progression of maize stomatal development in leaves**. Unexpanded maize leaves mature in a gradient with the developmentally youngest cells towards the base and the developmentally oldest cells towards the tip. **(A)** Stomatal complex formation is initiated by a transverse asymmetric division in a new stomatal row. **(B)** Pavement cells flanking the GMC acquire a SMC fate. At this stage, the nuclei are not yet polarized, but proteins (not shown) in the SMC may be polarized towards the GMC. **(C)** SMC nuclei polarize towards the GMC; preprophase band forms. **(D)** The SMCs divide, with each division forming **(D)** a subsidiary cell and a pavement cell. **(E)** The GMC undergoes an oriented, symmetric division symmetrically to form **(F)** the guard cell pair. Each stomatal complex is made of two subsidiary and two guard cells. Nuclei/DNA are shown in magenta; microtubule structures are shown in green. **(G)** Polarization of proteins in SMCs occurs in part B, and happens in an ordered sequence as shown.

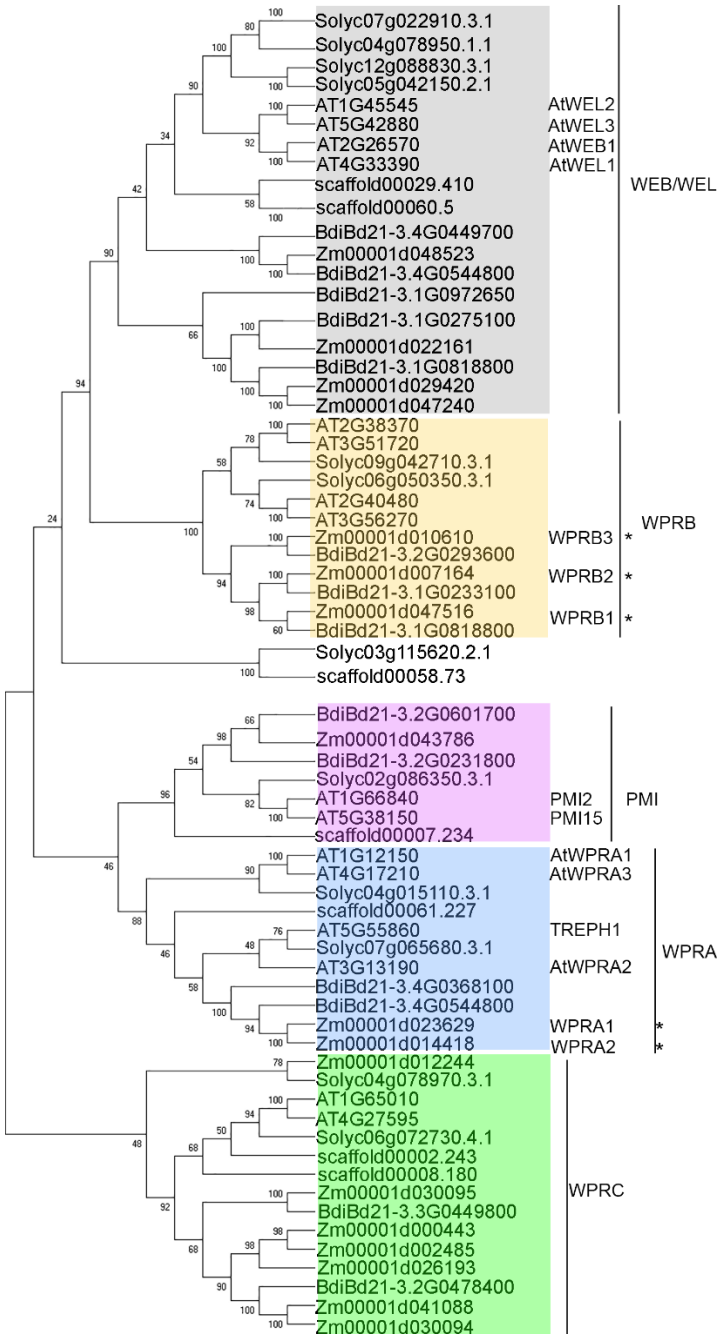


**Supplemental Figure 2. Protein tree of the WPR family in plants.** Protein coding sequences of WPR family members were identified from Phytozome 13 (https://phytozome-next.jgi.doe.gov/) from *A. thaliana* (dicot), *Amborella trichopoda* (dicot), *Solanum lycopersicum* (tomato, dicot), *B. distachyon* (monocot) and *Zea mays* (maize, monocot), and a protein tree was inferred. The proteins fall into 5 subfamilies, including the previously identified WEB/WEL, WPRB, WPRA and PMI clades – we also identified an additional WPRC clade. Previously named proteins are listed WEB1: WEAK CHLOROPLAST MOVEMENT UNDER BLUE LIGHT 1; WEB1-like proteins (WEL1, WEL2, and WEL3). WPR: WEB1/PMI2-related(including WPRA, WPRB and WPRC); PMI2: PLASTID MOVEMENT IMPAIRED 2; Numbers at nodes represent the percentage values given by 1000 bootstrap analysis samples. At: *Arabidopsis thaliana*, Zm: *Zea mays*. Bd: *Brachypodium distachyon,* Solyc: *Solanum lycopersicum*, scaffold: Amborella trichopoda. Asterisks mark proteins characterized in this study.

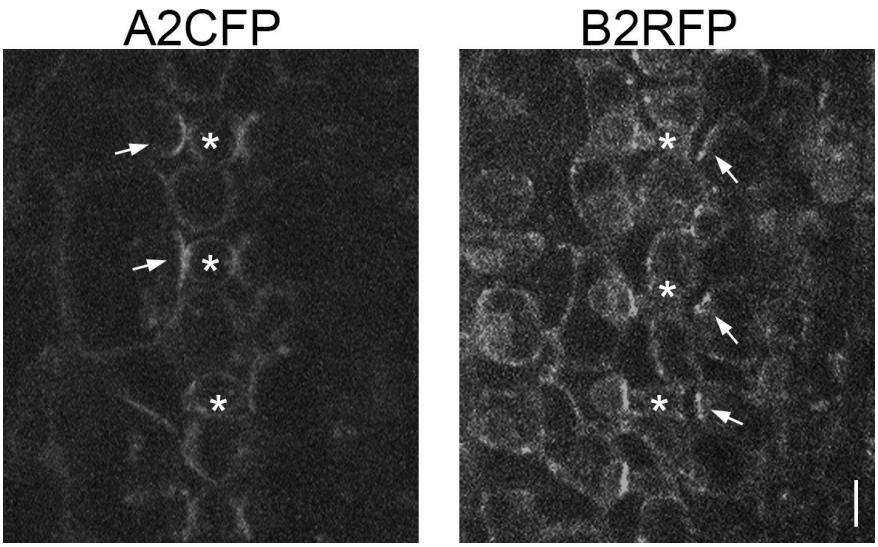


**Supplemental Figure 3**. **Plasmolysis assays of WPRA2-CFP and WPRB2-RFP transgenic plants.** Arrows indicate WPRA2–CFP or WPRB2-RFP enrichment in SMC which separated with GMC after 0.8M mannitol treatment. Asterisks indicate GMCs. Scale bar = 10 µm.

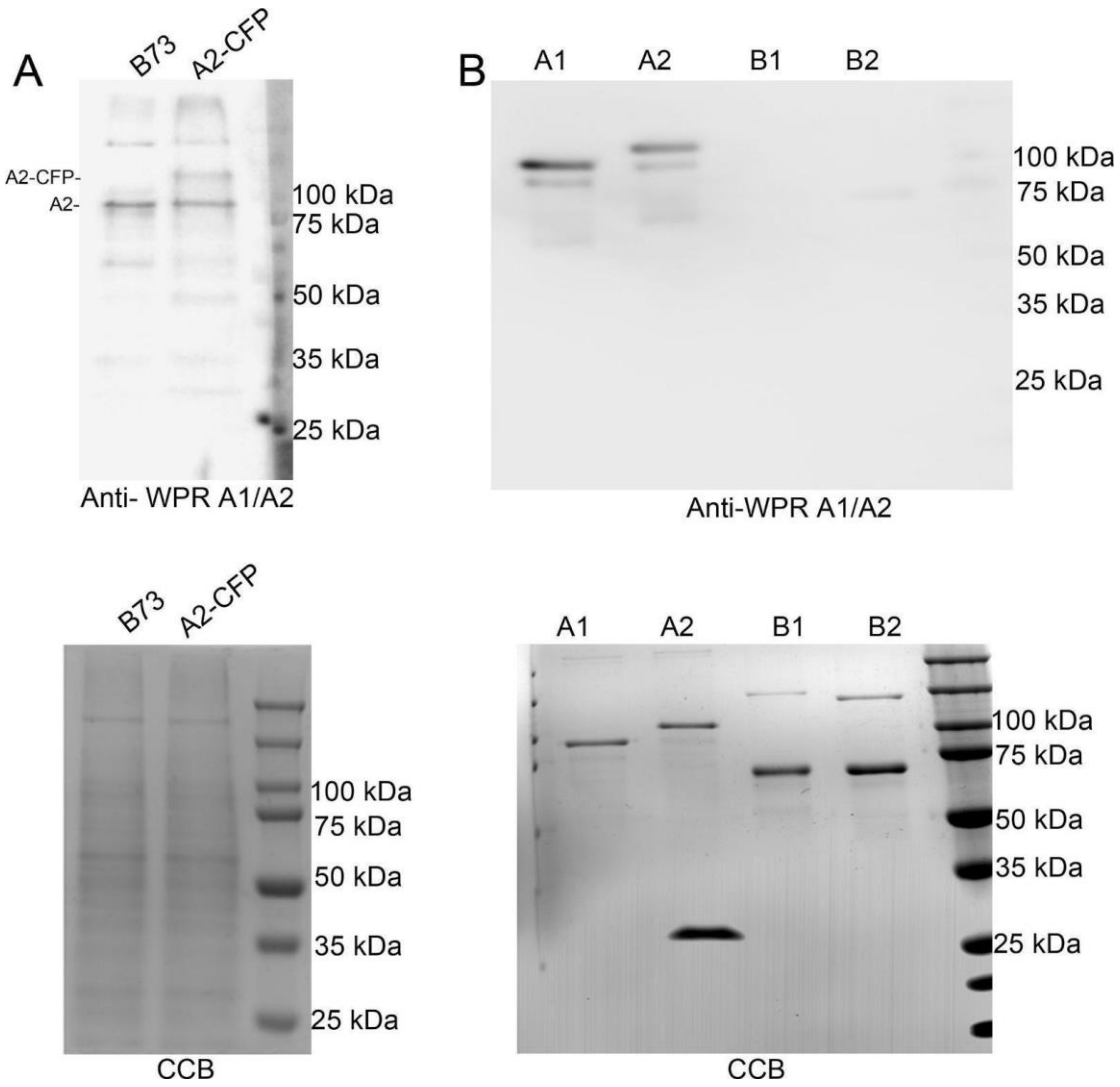


**Supplemental Figure 4**: **Confirmation of anti-WPRA1/A2 specificity using Western blotting.** **(A)** Western blot of proteins extracted from B73 and WPRA2-CFP transgenic plants probed with affinity-purified anti-WPRA1/A2. A band corresponding to the predicted size of endogenous WPRA1/A2 was recognized in B73. The same band was recognized in WPRA2-CFP expressing plants; as was a larger band specific to the transgenic plants, which corresponds to the predicted size of WPRA2-CFP. In lower panel, Coomassie blue (CCB) staining is shown as a loading control. **(B)** Western blot of bacterially-expressed and purified GST-tagged WPRA1, WPRA2, WPRB1, WPRB2 proteins probed with affinity-purified WPRA1/A2 antibody demonstrates the specificity of this antibody for WPRA proteins. The Coomassie blue–stained gel in the lower panel shows the purified proteins of WPRA1, WPRA2, WPRB1, WPRB2.

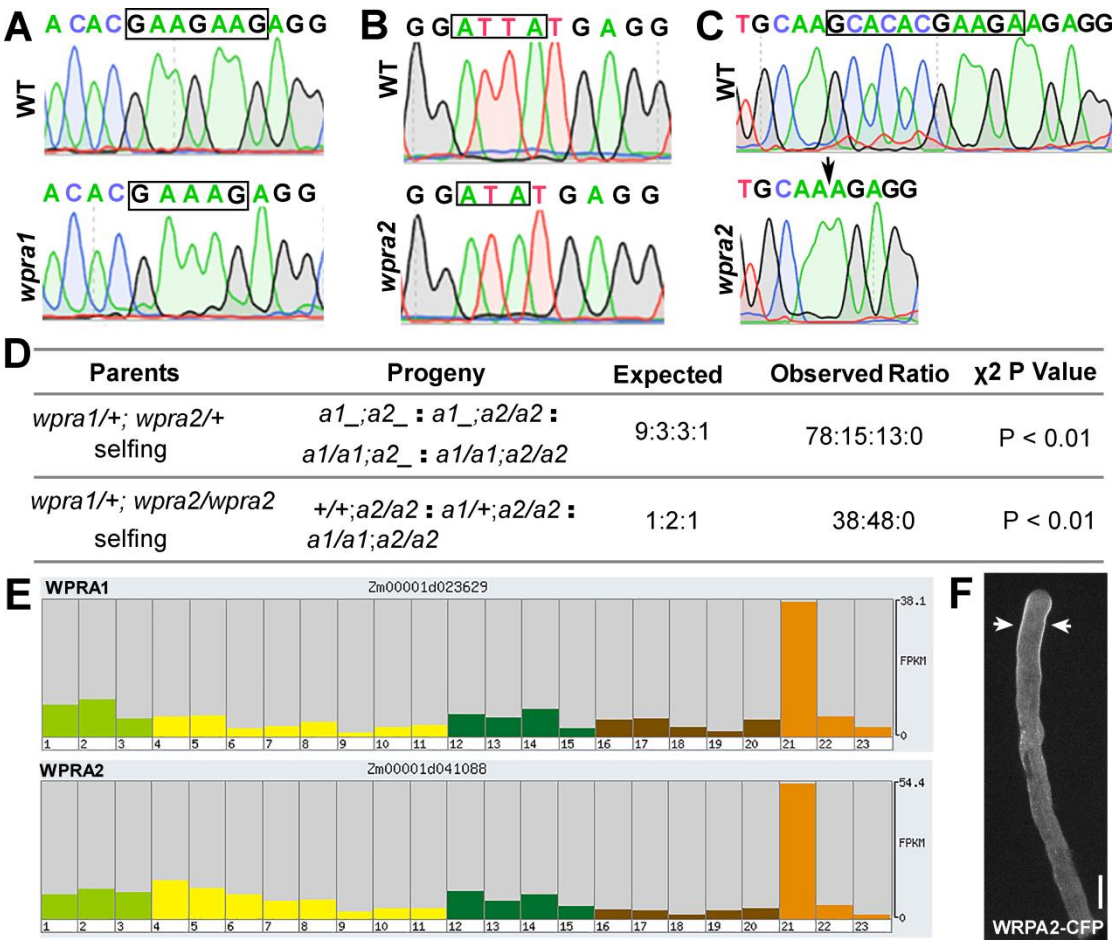


| Parents | Progeny | Expected | Observed Ratio | χ2 P Value |
|---|---|---|---|---|
| *wpra1/+; wpra2/+* selfing | *a1_;a2_* : *a1_;a2/a2* : *a1/a1;a2_* : *a1/a1;a2/a2* | 9:3:3:1 | 78:15:13:0 | P < 0.01 |
| *wpra1/+; wpra2/wpra2* selfing | *+/+;a2/a2* : *a1/+;a2/a2* : *a1/a1;a2/a2* | 1:2:1 | 38:48:0 | P < 0.01 |

**Supplemental Figure 5 CRISPR-Cas9 induced *Wpra1 and Wpra2* mutants have transmission defects.**

Mutated regions are labeled with black squares. **(A)** DNA sequences of Cas9-edited *Wpra1*. *wpra1* has a two nucleotide "GA" deletion at the gRNA2-targeted site. **(B)** and **(C)** DNA sequences of Cas9-edited *Wpra2.* Two mutations were identified: a "T" deletion was found at the gRNA1-targeted site (B), and an 11bp (GCACACGAAGA) deletion was found at gRNA2-targeted site (arrow, C). **(D)** Genotype analysis was performed in the progeny of *wpra1*/+; *wpra2*/+ and *wpra1*/+; *wpra2*/*wpra2* mutants. No *wpra1*/*wpra1*; *wpra2*/*wpra2* double mutants were recovered; observed ratios are significantly different from expected ratios. **(E)** RNA-seq expression level in maize growth stages (Data from MaizeGDB, Walley et al., 2016). Stage 21 is B73_Mature Pollen (expression level = 54.4). **(F)** WPRA2-CFP localization in maize pollen tube. Maize pollen stably expressing WPRA2-CFP were germinated in liquid culture for 1 hour at room temperature observed using spinning disk confocal and images were collected at × 60 objective (NA = 1.20, Olympus). The arrows point to subapex region localization of WPRA2-CFP. Scale bar in (F) = 10 µm.

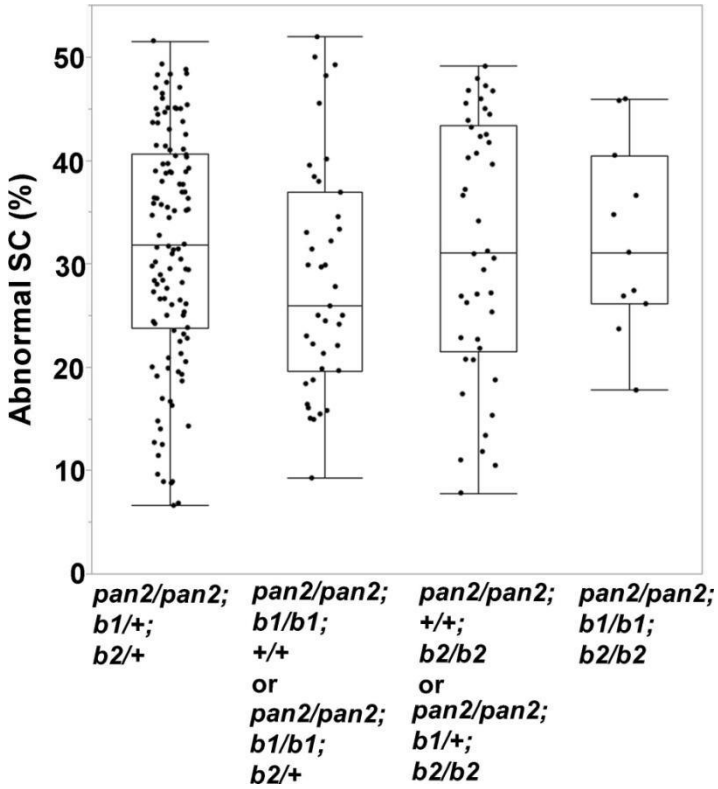


**Supplemental Figure 6. Mutations in *wprb1* and *wprb2* do not enhance *pan2*/*pan2* phenotype**

Stomatal phenotypes of progeny of *pan2*/*pan2; wprb1*/+*; wprb2*/+ plants were performed using the fully expanded third leaf. The percentage of abnormal subsidiary cell (SC) was quantified in different genotypes, *pan2/pan2; wprb1*/+*; wprb2/*+ (n = 113 plants), *pan2/pan2;wprb1*/*wprb1;wprb2_*(n = 38 plants), *pan2*/*pan2;wprb1_; wprb2*/*wprb2*(n= 41 plants) *and triple mutants pan2*/*pan2;wprb1*/*wprb1; wprb2*/*wprb2*(n= 11 plants). For each plant 100-200 subsidiary cells were genotyped. Student's T-tests were performed among these genotypes, no significant difference in these mutants.

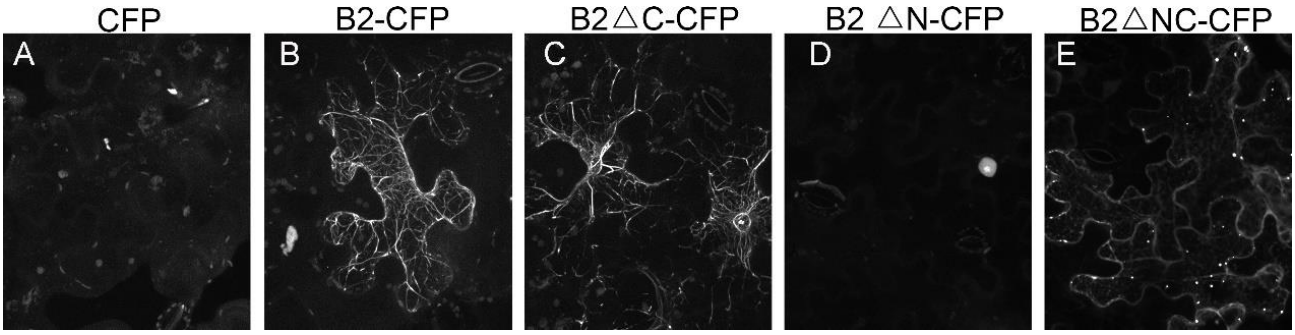


**Supplement Figure 7**. **Transient expression of WPRB2-CFP, and its truncated proteins.** Localization of WPRB2 in tobacco was confirmed using a CFP (rather than GFP) tag, and a C-terminal (rather than N-terminal) fusion. See Figure 6A for cartoon of protein truncations tested. (A) Soluble CFP. (B) Full length WPRB2-CFP. (C) C-terminal truncation WPRB2ΔC-CFP (D) N-terminal truncation WPRB2ΔN-CFP (E) Central DUF827 domain only WPRB2ΔNC. Filaments structures appears in WPRB2-CFP and WPRB2△C-CFP expressing tobacco cells, but not in WPRB2ΔN-CFP and WPRB2ΔNC-CFP expressing tobacco cells.

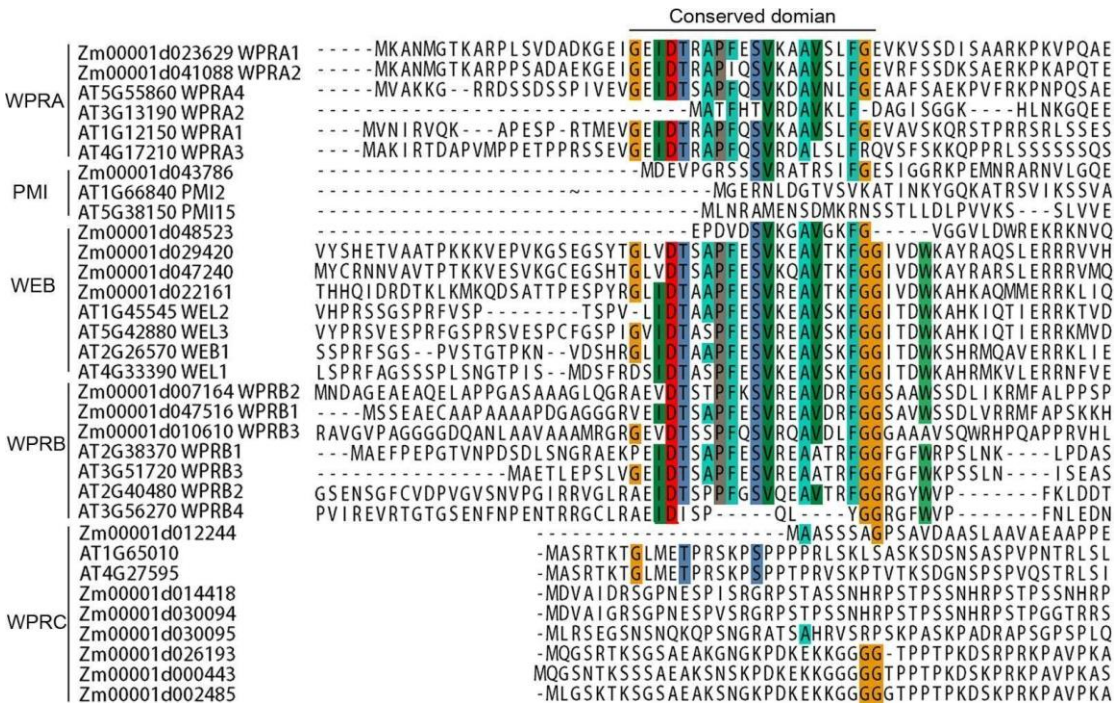


**Supplemental Figure 8. Alignment of the actin-binding domain of the WPR protein family.**

The N terminal amino acids sequence WPRs from *Arabidopsis* and maize were aligned using ClustalX 2.0.5 (Larkin et al., 2007) with the default settings.

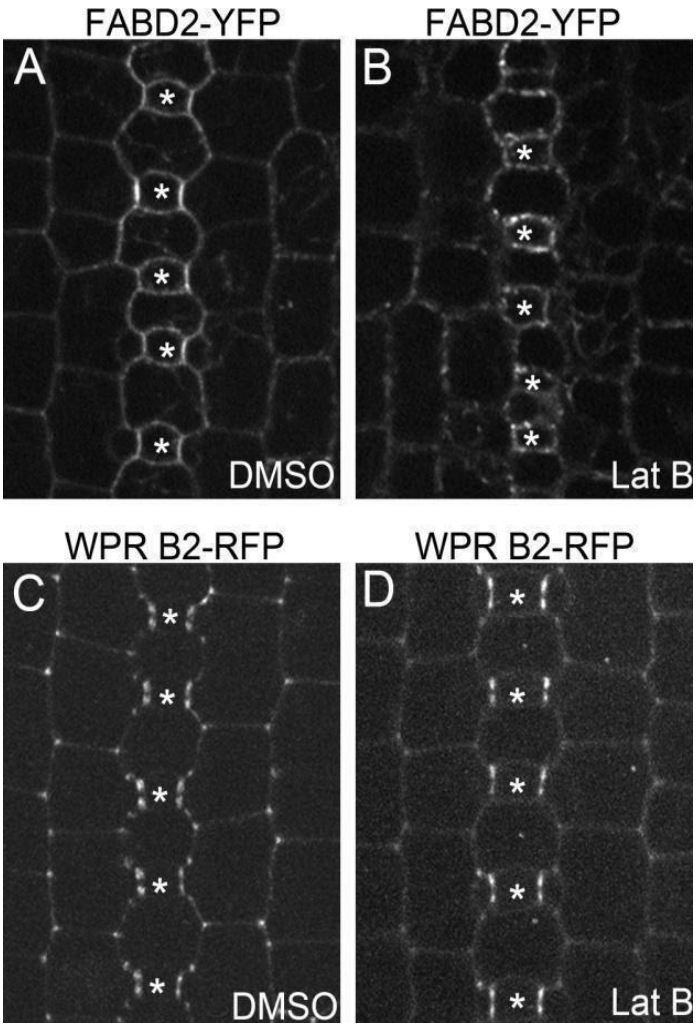


**Supplemental Figure 9**. **F-actin disruption does not affect the polarized localization of WPRB2-RFP in SMCs**.

**(A)** FABD2-YFP expressed maize leaves were treated with DMSO (negative control) and 40 µM Lat B for 4 hours. **(B)** WPRB2-RFP expressed maize leaves were treated with DMSO (negative control) and 40 µM Lat B for 4 hours. Asterisks mark GMCs.

| | WPRA2 | | | BRK1 | | | PAN2 | | | PAN1 | | | Actin | | |
|---|---|---|---|---|---|---|---|---|---|---|---|---|---|---|---|
| | WPRA 2-CFP only | WPRB 2-RFP only | Both | BRK1-CFP only | WPR only | Both | PAN2-YFP only | WPR only | Both | PAN1-YFP only | WPR only | Both | YFP-FABD2 only | WPR only | Both |
| WPRA 2-CFP | - | - | - | - | - | - | 0 | 0 | 254 | 0 | 0 | 286 | 0 | 67 | 140 |
| WPRB 2-RFP | 0 | 0 | 276 | 94 | 0 | 232 | - | - | - | - | - | - | - | - | - |

**Supplemental Table 1. Co-expression of polarized fluorescent protein markers in SMCs.** Quantification of cells in Figure 3. Leaf 4 of developing maize leaves, which were co-expressing two fluorescent proteins, were examined. The number of SMCs that had polarized accumulation at the SMC-GMC contact site quantified.

**Supplemental Table 2.** Primer sequences used in this study.

| Primer name | Sequence (5'-3') | Description |
|---|---|---|
| WPRA2-F | GGGGACA AGTTTGTACAAAAAAGCAGGCTGC ATAACCATTTTATGCTTCAAGC | Primers for *Wpra2* promoter and 5' UTR amplification |
| WPRA2-R | GGGG AC CAC TTT GTA CAA GAA AGC TGG GTA GAAGTTGCAATTACACCTCTTTGT | |
| WPRA2-P2 | GCTCCACCTCCACCTCCCATTTATTTAAATATTTTACGC | Primers for *Wpra2* coding region and 3' UTR amplification |
| WPRA2-P3 | GCTGCTGCGGCCGCTGGGGCCATGAAGGCAAATATGGGCAC | |
| WPRB2-F | GGGGACAAGTTTGAAAAAAGCAGGCTGCGAGATTCG AGACAACATACATG | Primers for *Wprb2* promoter and 5' UTR amplification |
| WPRB2-R | GGGGACCACTTTGTACAAGAAAGCTGGGTATAAAACT CTCACACGAGAGATAC | |
| WPRB2-P2 | GCTCCACCTCCACCTCCCATGGGGACTCGTGCCCCTCT | Primers for *Wprb2* coding region and 3' UTR amplification |
| WPRB2-P3 | GCTGCTGCGGCCGCTGGGGCCATGAACGACGCCGGCGAGGCC G | |
| Tag linker-F | ATGGGAGGTGGAGGTGGAGCT | Primers for CFP or RFP amplification |
| Tag linker-R | GGCCCCAGCGGCCGCAGCAGC | |
| WPRB2 topo-F | CACCATGAACGACGCCGGCGAGG | Primers for WPRB2N67 amplification |
| WPRB2N topo (1-67)-R | CTTTGGGCTCGGGGGCAGCG | |
| WPRB2N topo (1-142)-R | AGCGGCAGTGGGCAGCTCGGCTTG | WPRB2N142 R primer |
| WPRB2F-GW | GGGGACAAGTTTGTACAAAAAAGCAGGCTGCGC ATGAACGACGCCGGCGAGG | Primers for WPRB2 without stop code amplification |
| WPRB2R-GW(no stop code) | GGGGACCACTTTGTACAAGAAAGCTGGGTA ATGCGATCCCTTTTCCTTCTTC | |
| WPRB2 △N F-GW | GGGGACAAGTTTGTACAAAAAAGCAGGCTGC GCCGCTGAAGAGGTTGCAGAAG | Primers for WPRB2△C, WPRB2△N,WPRB2△NC amplification |
| WPRB2 △C R-GW | GGGGACCACTTTGTACAAGAAAGCTGGGTA CCTGTGTCCAGTCGTGGATCG | |
| WPRA1 topo-F | CACCATGAAGGCAAATATGGGC | Primers for WPRA1 CDS amplification |
| WPRA1 topo-R | TCACACAGATTTTTCCCCAGGAAG | |
| WPRA2 topo-F | CACCATGGGGTGGGGAAGAGCA | Primers for WPRA2 CDS amplification |
| WPRA2 topo-F | TTACACAGATTTTTCCCCAGGAAG | |

| | | |
|---|---|---|
| WPRB1 topo-F | CACCATGAGCTCCGAAGCAGAA | Primers for WPRB1 CDS amplification |
| WPRB1 topo-F | TTAAAAGGATTCTCTCTTCTT | |
| WPRB2 topo-F | CACCATGAACGACGCCGGCGAG | Primers for WPRB2 CDS amplification |
| WPRB2 topo-F | CTAATGCGATCCCTTTTC | |
| WPRB3 topo-F | CACC ATGGCGGAAGTGGCGGCGCGGC | Primers for WPRB3 CDS amplification |
| WPRB3 topo-R | GCTCAAGCCACCACGAGTGCAGGAG | |
| WPRA1 BamHI 63F | CGCGGATCC TTAGCCAAGGAGACAGA | Primers of WPRA1(63-503) amplification and GST-WPRA1 expression |
| WPRA1 EcorI 503R | CCGGAATTC CAACTTCTCTGACTC | |
| WPRA2 BamHI 63F | CGCGGATCC TTAGCCAAGGAGACAGA | Primers of WPRA1(63-570) amplification and GST-WPRA2 expression |
| WPRA2 E corI 570R | CCGGAATTC CTTCTCGCGCCATCT | |
| WPRB1 BamHI 73F | CGCGGATCC GCCGAGGAGCAGGCT | Primers of WPRB1(73-421) amplification and GST-WPRB1 expression |
| WPRB1 EcorI 421R | CCGGAATTC TTACCCGCTCTCAGATTT | |
| WPRB2 BamHI 78F | CGCGGATCC GAGGAGCAGACCGCG | Primers of WPRA1(78-429) amplification and GST-WPRB2 expression |
| WPRB2 EcorI 429R | CCGGAATTC GGATCGACATCTGCG | |
| WPRB2 BamHI F | CGCGGATCCATGAACGACGCCGGCGAG | Primers of WPRB2N240 amplification and GST-WPRB2N240 expression |
| WPRB2 N240 EcorI R | CCGGAATTCTTACTTCTGTGCAGTCCGGTTCAGCTC | |